Ancient TL

www.ancienttl.org · ISSN: 2693-0935

Issue 16(2) - December 1998
https://doi.org/10.26034/la.atl.v16.i2

Depletion of the quartz OSL signal using low photon energy stimulation

R. M. Bailey

Research Laboratory for Archaeology and the History of Art
University of Oxford, 6 Keble Road, Oxford, OX1 3QJ, UK.

(Received 8 April 1998 ; in final form 5 October 1998)

Abstract *For a given excitation photon energy, the rate of charge detrapping in quartz increases with sample temperature. This phenomenon is termed 'thermal assistance' and has been documented in a number of studies (see for example Spooner, 1994; Huntley et al., 1996; Bailey et al. 1997; Bailey 1998). An obvious consequence of this effect is that low photon energies can stimulate luminescence when sample temperature is sufficiently high. The work reported below assesses whether the signal observed from one particular quartz sample during low photon energy stimulation (at raised temperature) relates to the signal observed under blue+green stimulation. The possibility of inadvertent signal depletion due to laboratory 'safe lighting' is also discussed.*

Bleaching of quartz OSL using low energy photons

Since the appearance of the first published account of possible long wavelength stimulated luminescence from quartz, by Godfrey-Smith *et al.* in 1988 (measured at room temperature using combined 753 and 799 nm stimulation), a number of subsequent studies have produced a range of results. On the basis of emission spectra observations Huntley and Short (1992) attributed the IRSL measured in their sample (at ambient temperatures using diode stimulation centred on 950nm) not to quartz but to feldspar micro-inclusions. This conclusion is supported by the detailed bleaching spectra of Spooner (1994; ~400-900nm) where the bleaching rate of quartz was shown to be inversely related to illumination wavelength. Spooner (1994) showed that IR stimulation (~860nm) induced extremely low depletion rates, producing measurable luminescence only at temperatures greater than 70°C. Neither in this study nor in that of Bøtter-Jensen *et al* (1994; ~430-650nm) is there evidence of a long wavelength resonance, as exists in some feldspar samples at near infra-red wavelengths (Hütt *et al.*, 1988). In contrast to these findings Godfrey-Smith and Cada (1996) report the presence of an excitation resonance in quartz at similar wavelengths to the feldspar resonance (although there is the possibility, discounted by the authors, that this is indicative of significant feldspar microinclusions, as found by Huntley and Short in 1992).

In the present study, IR stimulation (using the IR-diodes mounted in a Risø-set, model TL-DA-12, emitting 875Δ80nm [1.30-1.56 eV] light at 40mW.cm^{-2} (Duller and Bøtter-Jensen, 1996)) yielded significant amounts of measurable luminescence from quartz only when the sample temperature was greater than 200°C. In light of the findings of Huntley and Short (1992), attempts were made to assess both sample purity (with respect to feldspar contamination) and the extent to which the luminescence observed under IR stimulation (at 220°C) related to the OSL signal measured when stimulating with the broad band blue+green light of the Risø-set (420-560nm [2.21-2.95 eV] at approximately 16 mW.cm^{-2}; Bøtter-Jensen and Duller, 1992).

For improved signal-to-noise ratios, a thermally sensitized sample was used (sample 317, a raised beach deposit from Tunisia - see Bailey 1998 for further details); annealing was at 650°C for 10 minutes in air. Preliminary experiments showed no significant difference between the results of annealed and non-annealed samples, with better precision achieved using thermally sensitised material. Two aliquots of the annealed quartz ('a' and 'b' respectively) were each given a β-dose of ~40Gy and preheated at 220°C for 300s. IRSL measurements of each aliquot (at 20°C), made immediately following preheating, yielded signals no higher than background levels, indicating an absence of significant feldspar contaminants. Aliquot 'a' was

subjected to seven repeated cycles, each consisting of a 0.1s OSL measurement at 20°C (blue+green stimulation) followed by 500s of IR stimulation at 220°C. Aliquot 'b' (the 'control') also went through seven cycles, each consisting of a similar 0.1s OSL measurement (20°C) and storage at 220°C for 500s (with no IR illumination). Aliquot 'b' was used to correct aliquot 'a' for thermal effects (thermal erosion of the signal and any sensitivity changes) and the loss of OSL due to repeated 0.1s measurements. The results of these measurements are shown in Figure 1.

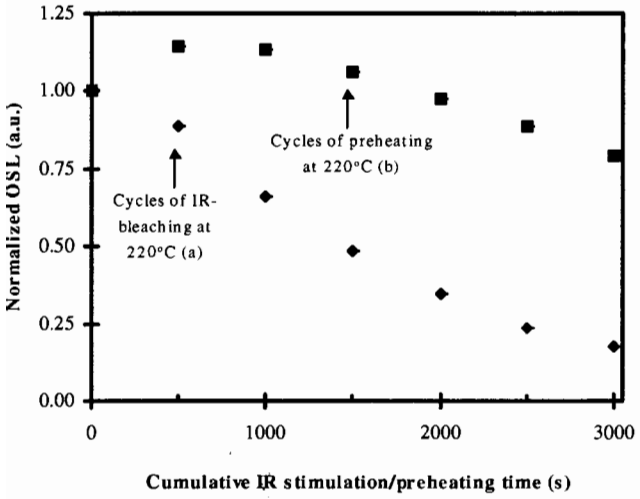

Figure 1.
Data set 'a': Raw OSL (minus background) remaining as a function of cumulative infra-red illumination at 220°C. Each data point represents the OSL observed during a 0.1s blue+green stimulation at 20°C (normalised to unity at t=0). The IRSL observed during each cycle is shown in Figure 3. Data set 'b': control aliquot for thermal effects. Standard errors are smaller than the size of the symbols in all cases. See main text for further details.

Successive 0.1s OSL measurements (blue+green excitation) suggest that IR stimulation at 220°C does indeed reduce the blue+green light stimulated signal (though at a much lower rate compared to the standard blue+green stimulation). Figure 2 shows the depletion after correction for measurement cycling and thermal effects. The data points are well fitted to a single exponential over the early part of the decay, to ~25 % of initial intensity, with a half-life of ~1,400s ($\lambda \approx 0.0005 s^{-1}$). The initial rise in the correction data (aliquot 'b') is attributed to thermal sensitisation not completed by the end of the initial preheat (following dosing). Further supporting evidence for the interpretation that IR stimulation at 220°C removes the OSL signal as monitored by the 0.1s measurements is illustrated in Figure 3, where the IRSL decay curves measured during each cycle are presented in series. Fitting an exponential decay yields a half-life for the IRSL decay indistinguishable from that obtained from the corrected 0.1s OSL measurements (Figure 2). Both the IRSL and the interposed 0.1s OSL (blue+green stimulation) both appear therefore to be measuring the same depletion of charge (recall that no IRSL was observed during 20°C measurements, indicating absence of feldspar contamination).

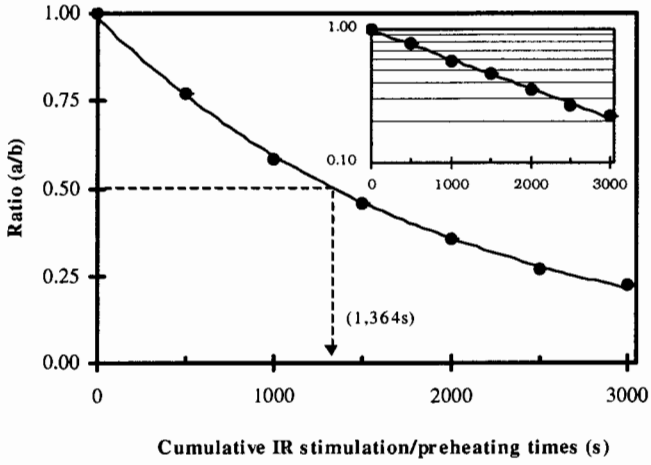

Figure 2.
Bleaching of the OSL signal (as monitored by 0.1s blue+green stimulated luminescence measurements) using IR-excitation at 220°C (data are corrected for thermal effects). 'a' and 'b' are as defined in Figure 1 and in the main text. The half-life of the fitted exponential decay is shown. Inset are the same data shown on a logarithmic vertical axis.

Relevance to laboratory safe-lighting

In order to minimise optical depletion of the dating signal during sample preparation, low photon energy lighting, typically in the ~600nm (~2 eV) region of the visible spectrum (orange, as listed by Aitken, 1998: Pg. ix) is commonly used for handling quartz. The observation reported above, that at raised temperature significantly less energetic IR stimulation (1.30-1.56 eV) substantially depletes quartz OSL, has a particular practical relevance to laboratory procedures. If samples exposed to laboratory 'safe-light' are at room temperature (~20°C) then depletion of the (blue+green stimulated) signal, over a period equal to the time needed for sample preparation and measurement is negligible (as observed in laboratory tests). However, in circumstances where sample temperature is considerably elevated (such as when

samples are taken from a preheat oven), exposure to the same lighting conditions may have detrimental effects (due to thermal assistance in the detrapping process).

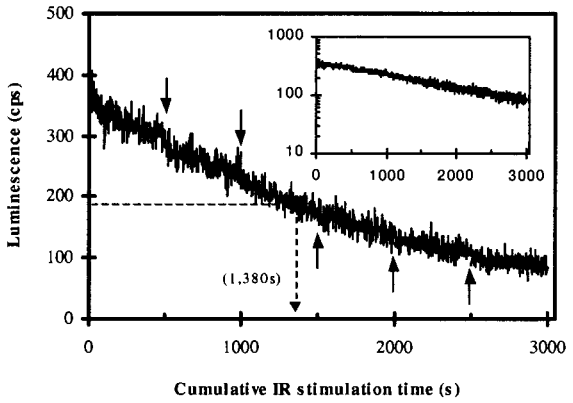

Figure 3.
Composite IRSL decay curve. Successive IRSL measurements (made at 220°C) are displayed in series against cumulative bleaching time, the beginning of each individual measurement marked by an arrow. Note that the half-life of the signal is indistinguishable from that shown in Figure 2.

An experiment was performed under what might be regarded as extreme conditions in order to gauge the likely maximum effect of 'safe-light-bleaching', as discussed above. Aliquots of naturally irradiated quartz (ca.120ka in age) were exposed to laboratory lighting for 10s at 220°C and cooled naturally to room temperature. For the purpose of this experiment, the laboratory was lit from a single 65W fluorescent tube filtered with two layers of 'Lee filters 158 Deep orange' celluloid (passing wavelengths greater than 540nm: 10% at ~560nm, 50% at ~605nm – information derived from spectral measurements), positioned approximately 1.5m vertically above the sample. Short (0.1s) OSL measurements were made both before and after 'safe-light' exposure. Once corrected for thermal effects and depletion due to measurement (using a separate aliquot that was not illuminated during heating), the signal depletion was approximately 3%, in each of two successive cycles. Clearly the induced depletion is not substantial but appears nonetheless to be present. For this reason, preheating in light-tight vessels and allowance of sufficient cooling time prior to exposure to 'safe-lighting' is advised.

Acknowledgements
I am very grateful to Professor Martin Aitken who in his role as referee provided an abundance of well targeted and helpful suggestions. I thank also Professor Ann Wintle for reading and commenting in a similar manner on an earlier version of the text.

References

Aitken M. J. (1998) An introduction to optical dating. Oxford science publications, Oxford University Press.

Bailey R. M (1998) The form of the optically stimulated luminescence signal of quartz: implications for dating. Unpublished Ph.D. thesis, University of London.

Bailey R. M., Smith B. W. and Rhodes E. J. (1997) Partial bleaching and the decay form characteristics of quartz OSL. *Radiation Measurements*, **27**, 123-136.

Bøtter-Jensen L. and Duller G. A. T. (1992) A new system for measuring optically stimulated luminescence from quartz samples. *Nuclear Tracks and Radiation Measurements*, **20**, 594-553.

Bøtter-Jensen L., Duller G.A.T. and Poolton N.R.J. (1994) Excitation and emission spectrometry of stimulated luminescence form quartz and feldspars. *Radiation Measurements*, **23**, 613-616.

Duller G.A.T. and Bøtter-Jensen L. (1996) Comparisons of optically stimulated luminescence signals from quartz using different stimulation wavelengths. *Radiation Measurements*, **26**, 603-609.

Godfrey-Smith D. I. and Cada M. (1996) IR stimulation spectroscopy of plagioclase and potassium feldspars, and quartz. *Radiation Protection Dosimetry*, **66**, 379-385.

Huntley D. J., Short M. A. and Dunphy K. (1996) Deep traps in quartz and their use for optical dating. *Can. J. Phys.*, **74**, 81-91.

Hütt G., Jaek I. and Tchonla J. (1988) Optical Dating: K-feldspars optical response stimulation spectra. *Quaternary Science Reviews*, **7**, 381-386.

Short M. A. and Huntley D. J. (1992) Infrared stimulation of quartz. *Ancient TL*, **10**, 19-21.

Spooner N. A. (1994) On the optical dating signal from quartz. *Radiation Measurements*, **23**, 593-600.

Reviewer
Martin Aitken

Comments :
I would like to underline the significance of Figs 1 - 3. As the author says, these results indicate that there is IR bleaching (at elevated temperature) of the traps responsible for the blue+green stimulated luminescence (BGSL) with a depletion-rate equal to that of the IRSL signal itself. This gives evidence that the BGSL and the IRSL are from the same traps --- which was not necessarily the case for the elevated temperature IRSL observed by Spooner (1994). It also confirms the absence of feldspar contamination; the absence of any above-background IRSL at 20°C is not sufficient to exclude the possibility that, due to thermal assistance, such contamination is responsible for the IRSL at elevated temperature.

Authors reply
I agree with the comments of the Reviewer.

Dose-rate conversion factors: update

Grzegorz Adamiec[1] and Martin Aitken[2]

[1]Research Laboratory for Archaeology, Oxford University, 6 Keble Road, Oxford OX1 3QJ, UK.
E-mail: grzegorz.adamiec@rlaha.ox.ac.uk
[2]Le Garret, 63 930 Augerolles, Puy-de-Dôme, France.
E-mail: martin.aitken@linacre.ox.ac.uk

(Received 6th June 1998 ; in final form 1st september 1998)

Abstract : *Dose-rate conversion factors relevant to luminescence and electron spin resonance dating have been derived from values for the energy carried by radiations emitted during nuclear transformations given in the current ENSDF (Evaluated Nuclear Structure Data File). For beta and gamma radiation the factors are a few percent lower than previously used. For the effective alpha dose-rate it is more appropriate to use an approach based on particle ranges and resultant values are given.*

Introduction

In trapped charge dating evaluation of dose-rate is of equal importance to that of palaeodose. In most approaches the dose-rate is derived from measurement of radioelement concentration (or activity) by means of conversion factors, and because these factors are outside the ken of the dating specialist there is a tendency to take them for granted as written in stone. In fact they are based on nuclear data tables and these are in an on-going process of refinement. The tables are dauntingly complex and fortunately for the dating communities a formulation is available in which values for the radiation components of the energy release are given specifically from the dosimetry point of view. The overall tables are known as the *Evaluated Nuclear Structure Data File* (ENSDF) and the dosimetry-orientated formulation known as the Medical Internal Radiation Dose (MIRD) format. These are available on the Brookhaven National Laboratory Web site (http://www.nndc.bnl.gov.) and the International Atomic Energy Authority Web site (http://www-nds.iaea.or.at); except for Table 7 and part of Table 8, the values of the present paper are based on MIRD downloaded on 22nd June 1998. Details about ENSDF has been given by Martin & Blickert-Toft (1970) and by Burrows (1998).

Earlier use of ENSDF was made by Nambi & Aitken (1986) through the dosimetry-orientated format published by the International Commission on Radiation Protection as ICRP-38. Comparison with the values of Nambi & Aitken (1986) is summarized in Tables 4 and 8; since ICRP-38 was based on ENSDF as of 1978 it is not surprizing that there are differences. Prior use of nuclear data tables has been made by Aitken (1974), Aitken & Bowman (1975), Bell (1976, 1977, and 1979), Carriveau & Troka (1978). Subsequent to Nambi & Aitken (1986), re-assessments have been made by Liritzis & Kokkoris (1992) and by Ogoh *et al.* (1993), as discussed in Appendix A.

The paper is primarily written with luminescence dating in mind but it is largely applicable to dating by electron spin resonance as well.

The data

Tables 1, 2 & 3 show the energy emission values and half-lives obtained from the Brookhaven Web site mentioned above for the three radioactive series; Table 4 gives comparison between these data and those presented by Nambi & Aitken (1986). As will be seen there are appreciable decreases in the totals for beta radiation and gamma radiation from the Th-232 series, the principal contributor to these decreases being Ac-228. It is not easy to pinpoint particular measurements that are responsible for decreases; this is because the values are usually based on comprehensive schemes of nuclear energy levels incorporating a number of relevant measurements rather than on single direct measurements.

In Table 5 the emission values have been converted into dose-rate. This is on the usual infinite matrix assumption that the dose-rate is equal to the rate of energy emission per unit mass, implying that there is homogeneity both in radioactive content and

in absorption coefficient. The value given for 'full series' is for the case of radioactive equilibrium, i.e. the disintegration rate of each daughter is equal to that of the parent, except where modified by branching; the value labelled 'pre-Rn' corresponds to 100% escape of radon from the two principal series. This and other types of disequilibrium have been discussed by Krbetschek *et al.* (1994) and Olley *et al.* (1996), among others.

Data for potassium and rubidium are given in Table 6. For potassium, the value for gamma radiation is unchanged from that of Nambi & Aitken (1986) but the value for beta radiation is lower by 4%. For rubidium the beta value is lower by a factor of 1.26; however, except for the internal dose-rate in coarse grains of potassium feldspar, the change is unimportant. The concentration ratio of 200:1 between potassium and rubidium used in Table 6 is an arbitrary choice that is within the range of ratios encountered in samples.

The alpha particle contribution

The luminescence induced by alpha particles per gray of deposited energy is dependent on particle energy, decreasing as the particle energy decreases; this is in contrast to the case for the lightly-ionizing radiations, beta and gamma, for which the effectiveness is independent of energy. Thus in the *k*-value system, developed by Zimmerman (1971), it is necessary to know the precise energy of the alpha particles used for measuring *k* (the ratio of alpha effectiveness compared to that of beta or gamma radiation, effectiveness being the luminescence induced per gray) and also to make allowance for that fact that the alpha particles received during burial have a spectrum that spreads from zero to 8.8 MeV. To do this Zimmerman (1971) introduced *k*(effective) which for quartz he calculated, on the basis of range-energy data then available, as being less than *k*(3.7 MeV) by a factor of 0.86 for the thorium series and 0.80 for the uranium series.

It was implicit in the results of Zimmerman (1971) that, to a first approximation, the luminescence induced per unit length of alpha particle track is independent of particle energy. This was confirmed by Bowman (1976) using the alpha beam from a Van de Graaff generator and in respect of ESR by Lyons & Brennan (1989). This approximation is the basis of the three track-length approaches: the *a*-value system (Aitken & Bowman 1975), the *b*-value system (Bowman & Huntley 1984), and the omnidirectional flux system (Valladas & Valladas 1982). Because the alpha count-rate from a thick layer of sample is proportional to the length of track generated in the sample by its constituent thorium and uranium series this count-rate can be used to give direct determination of the alpha dose-rate during burial. Also required is measurement, for the sample concerned, of the luminescence induced by unit length of track from an artificial source. By comparing this luminescence with that induced per gray of beta (or gamma) radiation, alpha count-rate can be converted to effective alpha dose-rate (see Appendix B). It is 'effective' in the sense of being appropriate for use in the usual age equation in which the palaeodose is expressed in terms of grays of beta (or gamma) radiation.

Although the track-length approaches are conceptually more difficult than the *k*-value system, the latter has the basic disadvantage that there is a need to have an accurate knowledge of the particle energy used in measurement of sample sensitivity. It is not just a matter of energy of the particles emerging from the alpha source; strictly, allowance should also be made for the degradation in energy as the particles penetrate the sample. Hence the preferred values for the effective alpha contribution are those based on track-length as given in Table 7.

Concluding remarks

Although the 8% decrease in the gamma dose-rate from the thorium series is substantial, there is considerable dilution when an actual context is considered, as illustrated in the example of Table 8. For fine-grain dating the total dose-rate is 2.11 according to the present paper compared to 2.18 according to Nambi and Aitken (1986), a decrease of 3%. For coarse-grain dating the values are 1.60 and 1.65 respectively, a decrease of 3% as well. For contexts in which there is dominance by thorium or potassium, the decreases will be greater.

A historical survey of some published conversion factors is given in Appendix A. It will be seen that, for the specimen context of Table 8 at any rate, the totals of the present paper are a few percent lower than all previous ones. However there is no case for diluting the present factors by averaging because the earlier assessments are essentially based on the progenitors of the present ENSDF and these are now superceded. It is reassuring to note that, at any rate for contexts not too dissimilar to the specimen one considered, no dramatic revision is needed in respect of ages based on earlier conversion factors: the highest fine-grain totals, those of Aitken (1974) and Bell (1979), are some 4% higher than that for the present paper; the highest coarse-grain total, that of Aitken (1974) is some 6% higher.

Of course, there are other influences on dose-rate accuracy besides the basic conversion factors, such as related to moisture content, grain-size, radioactive disequilibrium etc. These tend to introduce an uncertainty that is dominant and so the shifts consequent on changing to the factors of the present paper will usually be contained within error limits. Nevertheless, the case for utilization of these factors is just as strong as the case for using state-of-the-art refinements in palaeodose determination. To do otherwise runs the risk of drifting into a situation where there will be two ages for a sample, one based on 'set in stone' factors and another based on the best available data from nuclear physics.

Acknowledgements

We are sincerely grateful to Dr. T. W. Burrows of the Brookhaven National Laboratory for his patient explanation to us of various features of ENSDF. In addition, all of us in trapped charge dating owe an immense debt of gratitude to the multitude of nuclear physicists on whose work ENSDF is based.

G.A. would like to express his gratitude to the Research Laboratory for Archaeology and the History of Art and to the Overseas Research Students Awards Scheme for supporting his work.

Finally, we are appreciative of a number of valuable suggestions made by the Reviewer.

Table 1: Energy release in the Th-232 decay series

Isotope	Half-life	Alpha	Beta	Gamma
Th-232	14.05 Ga	4.00	-	$<5x10^{-4}$
Ra-228	5.75 a	-	0.01	0.001
Ac-228	6.15 h	-	0.413	0.854
Th-228	1.91 d	5.31	0.019	0.003
Ra-224	3.66 d	5.57	0.002	0.010
Rn-220	55.6 s	6.28	-	0.001
Po-216	0.145 s	6.77	-	$<5x10^{-4}$
Pb-212	10.6 h	-	0.173	0.144
Bi-212	60.6 m	2.14	0.502	0.103
Po-212 (0.641)	0.299 ms	5.63	-	-
Tl-208 (0.359)	3.05 m	-	0.209	1.205
Total		35.7	1.33	2.32
Pre-Rn total		14.9	0.444	0.868

Notes for Table 1

1. Energies are given in MeV and represent the energy emitted per disintegration.
2. Non-SI units used in half-lives: 1a=1 year; 1d=1 day; 1 h=1 hour; 1 m=1 minute
3. Branching ratios are shown in parenthesis against the radioelements in the branches; associated values given for energy release are after adjustment for branching. Note that the branching also affects the energy release of the radioelement at which the bifurcation occurs; thus the value given for the alpha release by Bi-212 is 35.9% of the full energy --- because Tl-208 is formed by alpha emission from Bi-212.
4. Internal conversion and Auger electrons are included with the beta component (which is the average beta energy rather than the maximum). X-rays and annihilation radiation are included with the gamma component. Alpha recoil energies have not been included; this is on the basis that the contribution to luminescence will be negligible on account of the resultant ionization density being even higher than for the alpha particles themselves; the total recoil energy does not exceed 2% of the alpha total for any series. Neutrinos have been ignored because of their very low absorption in matter.
5. A dash indicates that no radiations of that type are listed in MIRD.
6. At-216 has been omitted since its contribution to the total energy is insignificant.

Table 2: Energy release in the U-238 decay series.

Isotope	Half-life	Alpha	Beta	Gamma
U-238	4.468 Ga	4.19	0.007	0.0011
Th-234	24.1 d	-	0.060	0.0093
Pa-234m	1.17 m	-	0.818	0.0161
Pa-234 (0.0016)	6.75 h	-	0.001	0.0023
U-234	246 ka	4.68	0.012	0.0015
Th-230	75.4 ka	4.58	0.013	0.0014
Ra-226	1600 a	4.77	0.0038	0.0074
Rn-222	3.82 d	5.49	-	0.0004
Po-218	3.11 m	6.00	-	-
Pb-214	26.8 m	-	0.294	0.2521
Bi-214	19.9 m	<0.005	0.652	1.4814
Po-214	164 ms	7.68	$<5x10^{-4}$	0.0001
Pb-210	22.3 a		0.033	0.0047
Bi-210	5.01 d	<0.005	0.389	-
Po-210	138.4 d	5.31	$<5x10^{-4}$	$<5x10^{-5}$
Total		42.7	2.28	1.78
Pre-Rn total		18.2	0.906	0.037

Notes for Table 2

1. See notes 1-5 of Table 1.

2. At-218, Rn-218, Tl-210 and Tl-206 have been omitted since their contribution to the total is insignificant

Table 3: Energy release in the U-235 decay series.

Isotope	Half-life	Alpha	Beta	Gamma
U-235	704 Ma	4.27	0.037	0.180
Th-231	25.5 h	-	0.1506	0.028
Pa-231	32.8 ka	4.84	0.032	0.040
Ac-227	21.8 a	0.07	$<5x10^{-4}$	$<5x10^{-4}$
Th-227 (0.986)	18.7 d	5.70	0.028	0.108
Fr-223 (0.014)	21.8 m	-	0.006	0.001
Ra-223	11.4 d	5.67	0.066	0.137
Rn-219	3.96 s	6.63	0.007	0.058
Po-215	1.78 ms	7.39	-	$<5x10^{-4}$
Pb-211	36.1 m	<0.005	0.455	0.064
Bi-211	2.14 m	6.54	0.001	0.047
Tl-207 (0.997)	4.77 m	-	0.494	0.002
Total		41.1	1.27	0.665
Pre-Rn total		20.6	0.319	0.493

Notes for Table 3

1. See notes 1-5 of Table 1.
2. At-215 and Po-211 have been omitted since their contribution to the total is insignificant.

Table 4: Main differences between the current energy per disintegration values and the data presented by Nambi & Aitken (1986).

Isotope	Alpha	Beta	Gamma
Th-232 series:			
Th-232	·	-0.9%	·
Ra-228	·	-0.5%	·
Ac-228	·	-4.5%	-4.6%
Bi-212	·	+2.2%	-3.3%
Total	-0.7%	-4.4	-8.3%
U-238 series:			
Bi-214	·	·	-1.5%
Total	-0.4%	-1.2%	-1.2%
U-235 series:			
Total	-1.2%	-8.6%	+5.6%

Notes for Table 4

1. Percentages are with respect to the total for the radiation type concerned of the series using Nambi & Aitken (1986) values as base. All are decreases except for the beta emission from Bi-212, and the gamma from the U-235 series
2. The only individual isotopes shown are those which contribute more than 0.5% change in the total for the radiation type of the series.

Table 5: Dose-rate data for the thorium and uranium series

	Th-232	**U-238**	**U-235**	**Nat. U**
1. Abundance by weight	100%	99.29%	0.71%	-
2. Half-life [Ga]	14.05	4.468	0.704	-
3. Parent activity [Bq mg^{-1}]	4.06	12.4	80	12.9
4. Activity share in nat. U	-	95.6%	4.4%	-
Dose-rate [Gy ka^{-1}] per ppm				
5. alpha, full series	0.732	2.685	16.6	2.78
6. alpha, pre-Rn	0.305	1.146	(16.6)	1.26
7. beta, full series	0.0273	0.143	0.515	0.146
8. beta, pre-Rn	0.0091	0.057	(0.515)	0.060
9. gamma, full series	0.0476	0.112	0.269	0.113
10. gamma, pre-Rn	0.0178	0.0025	(0.269)	0.0044
To obtain dose-rate [Gy ka^{-1}] per unit specific activity of parent [Bq kg^{-1}]				
11. Divide lines 5-10 by	4.06	12.4	80	12.9

Notes for Table 5

1. The rows labelled 'pre-Rn' give the values for 100% escape of radon in the case of the Th-232 and U-238 series, but because of the short half-life of Rn-219 the values given for U-235 and natural U include contributions of that gas and its daughters.

2. Dose-rate values are based on Table 1, 2 and 3.

3. 'ppm' equals mg of parent per kg of sample.

4. The weight abundances given in row 1 for U-238 and U-235 correspond to the natural atomic abundances of 99.28% and 0.72% respectively.

Table 6: Dose-rate data for potassium and rubidium

	K-40	**Rb-87**
1. Natural abundance [mg/g]	0.119	283
2. Half-life [Ga]	1.277	47.5
3. Average energy per disintegration [MeV]	β: 0.501 γ: 0.156	β: 0.082
4. Specific activity [Bq kg^{-1}] for concentration of 1% natural K and 50 ppm natural Rb	β: 270 γ: 32.5	β: 45.29
5. Dose-rate [Gy ka^{-1}] for concentrations as in 4	β: 0.782 γ: 0.243	β: 0.019
6. As in 5 but for 1% K_2O and 50 ppm Rb_2O	β: 0.649 γ: 0.202	β: 0.017

Notes for Table 6

1. The energy given is that released per disintegration, i.e. after allowance for branching between beta and gamma (89.3% and 10.7% respectively).
2. The contents given in row 1 correspond to natural atomic abundances of 116.7 ppm and 27.8%.

Table 7: Alpha particle data and effective dose-rates

	Th-232	U-238	U-235	nat. U
Average alpha ranges [μg mm^{-2}]:				
1. Full series	67.4	56.7	65.9	-
2. pre-Rn	51.2	44.6	(65.9)	-
Effective number of full alpha emissions per parent disintegration:				
3. Full series	6	8	7	-
4. pre-Rn	3	4	(7)	-
Count-rate [ks^{-1}] per [Bq kg^{-1}] of parent, 42-mm diameter scintillator:				
5. Full series	0.119	0.129	0.136	0.129
6. pre-Rn	0.0426	0.0482	(0.136)	0.0521
Count-rate [ks^{-1}] for 1 ppm of parent, 42-mm diameter scintillator:				
7. Full series	0.483	1.60	10.9	1.67
8. pre-Rn	0.173	0.599	(10.9)	0.672
Share of counts in natural uranium				
9. Full series		95.4%	4.6%	
10. pre-Rn		88.5%	11.5%	
Dose-rate [Gy ka^{-1}] for count-rate = 10 ks^{-1}, 42-mm diameter scintillator:				
11. Effective α, a=0.1, full series	1.26	1.31	1.26	1.31
12. Effective α, a=0.1, pre-Rn	1.31	1.35	(1.26)	1.34
13. beta, full series	0.565	0.893	0.475	0.874
14. beta, pre-Rn	0.528	0.951	(0.475)	0.896
15. gamma, full series	0.986	0.697	0.248	0.676
16. gamma, pre-Rn	1.03	0.0387	(0.248)	0.0627
Effective alpha dose-rate [Gy ka^{-1}] per 1 ppm of parent, a = 0.1:				
17. Full series	0.0611	0.210	1.37	0.218
18. pre-Rn	0.0227	0.0808	(1.37)	0.090

Notes for Table 7

1. The ranges were obtained by adding 2% to the ranges evaluated for quartz by Brennan & Lyons (1989) using the data of Ziegler *et al.* (1985); the extra 2% makes allowance for the higher average atomic weight to be expected in typical sediment. For the pottery composition considered by Brennan & Lyons (1989) the ranges were 5% greater than for quartz. No adjustment in range has been made on account of the slightly different alpha energies noted in Table 4.

2. The range values given by Aitken (1998) are between 6% and 7% higher than those given in the Table. This is on account of use by that author of the values given by Valladas (1988) which were based on Zeigler (1977) rather than Zeigler *et al.* (1985). There are corresponding differences in subsequent count-rates and dose-rates but the effective alpha dose-rates per unit count-rate are not affected because both are proportional to range.

3. The count-rates are for a sample that is alpha-thick and for a scintillator with an area of 13.85 cm^2. It is assumed that the efficiency of the scintillator is 100%, i.e.that every incident particle gives rise to an output pulse from the

photomultiplier; however it should be noted that studies by Woithe & Prescott (1995) indicate that the efficiency of a typical ZnS screen may be only about 90%.

4. The assumed electronic threshhold setting is such that for a sample containing only the Th-232 series, 85% of the pulses from the photomultiplier are recorded; with this setting the corresponding values are 82% for U-238 and 85% for U-235; for the pre-Rn parts of the first two series the values are 80% and 78% respectively.

5. Rows 13-16 utilize the data of rows 7 and 8 together with the data of Table 5, but rows 11, 12, 17, and 18 are based on the a-value system; for the b-value system, note that $b = 13a$ when the units of b are Gy μm^2. Values of 0.90 and 0.88, for the full series and for the pre-Rn parts respectively, have been used for η, the efficiency factor (see Appendix B).

Table 8 Comparative dose-rates [Gy ka^{-1}] for a specimen context

		Dose-rates				
	Concentration	**effective alpha**	**beta**	**gamma**	**Fine-grain total**	**Coarse grain total**
K	1%	-	0.782 (0.814)	0.243 (0.243)	1.025 (1.058)	0.947 (0.976)
Rb	50 ppm	-	0.019 (0.023)	-	0.019 (0023)	0.014 (0.018)
Th	3 ppm	0.183 (0.190)	0.082 (0.086)	0.143 (0.156)	0.408 (0.433)	0.217 (0.234)
Nat. U	1 ppm	0.218 (0.222)	0.146 (0.147)	0.113 (0.114)	0.477 (0.489)	0.244 (0.246)
Cosmic	-	-	-	0.18	0.18	0.18
Totals	-	0.401 (0.413)	1.029 (1.071)	0.679 (0.693)	2.11 (2.18)	1.60 (1.65)

Notes for Table 8

1. The values are those from Tables 5, 6, and 7 of the present paper and from Tables 4 and 5 of Nambi & Aitken (1986), the latter being in parenthesis. The effective alpha dose-rates for the former are for $a = 0.1$ (as in Table 7) and those for the latter are derived using $k = 0.1$ and conversion factors to k(effective) of 0.86 and 0.80 for Th and U respectively.

2. Since it is highly penetrating it is convenient to list cosmic radiation under 'gamma'. The value quoted is appropriate to a depth of a metre.

3. In the totals for coarse-grain dating an attenuation factor of 0.90 has been used for the beta contributions except in the case of Rb for which the factor has been arbitrarily taken to be 0.75 on account of the lower penetration (appropriate evaluation of this factor is not available).

4. The moisture content is assumed to be zero.

Appendix A : Historical survey

Table A.1 gives values for the specimen context of Table 8 based on conversion factors published from 1974 onwards; the publications listed have been restricted to those that embody a primary assessment of nuclear data tables.

It should be noted that the date of the publication is often somewhat later than that of the nuclear data tables on which the factors are based; thus the source data for Aitken (1974) were from tables of 1967, those for Nambi & Aitken (1986) were from ENSDF as at 1978, and the sources used by Liritzis & Kokkoris (1992) have publication dates of 1983 and 1986. As noted earlier the source data for the present paper are from ENSDF as at mid-1998; hence the source data span three decades and the consistency is remarkable.

Table A.1: Annual dose-rates in [Gy ka^{-1}] for a specimen context: historical summary

K: 1%	Rb: 50 ppm	Th: 3ppm	U: 1ppm	Total fine	Total coarse
Aitken (1974)					
1.122	-	0.445	0.456	2.20	
1.035	-	0.259	0.225		1.70
Aitken & Bowman (1975)					
1.106	-	0.412	0.470	2.17	
1.019	-	0.216	0.232		1.65
Bell (1976)					
1.069	-	0.428	0.501	2.18	
0.986	-	0.228	0.259		1.65
Bell (1977)					
1.069	-	0.430	0.489	2.17	
0.986	-	0.231	0.246		1.64
Bell (1979)					
1.080	0.025	0.430	0.489	2.21	
0.997	0.019	0.231	0.246		1.67
Carriveau & Troka (1978)					
1.050	0.019	0.407	0.498	2.16	
0.970	0.014	0.209	0.255		1.63
Nambi & Aitken (1986)					
1.058	0.023	0.433	0.489	2.18	
0.976	0.018	0.234	0.246		1.65
Liritzis & Kokkoris (1992)					
1.068	0.025	0.422	0.490	2.19	
0.986	0.019	0.226	0.243		1.65
Adamiec & Aitken (1998)					
1.025	0.019	0.408	0.477	2.11	
0.947	0.014	0.217	0.244		1.60

Notes for Table A.1

1. The values are for the same specimen context as for those of Table 8, with the same parameters. As in that table the totals include a cosmic-ray contribution of 0.18 Gy/ka.
2. The first row under each publication is for fine-grain dating and the second for coarse-grain dating.
3. Conversion factors have also been derived by Ogoh *et al.* (1993) using the basic data of Liritzis & Kokkoris (1992). The factors derived are within 1% of those of the latter except that the alpha dose-rate from uranium is lower by 1.4% and the beta dose-rate from rubidium is higher by 1.7%. The resultant values appropriate to Table A.1 are all within 1% of those of Liritzis & Kokkoris (1992) except in respect of rubidium.

Appendix B : Conversion of various entities

Below we give the expressions which were used to calculate and convert various values used in this paper.

1) **Conversion of oxide content to elemental content**

Table B.1: Conversion of weight content: oxide to element

Oxide	Element	Atomic weight	Equivalent element content
K_2O	K	39.10	0.8301
Rb_2O	Rb	85.5	0.9144
ThO_2	Th	232.0	0.8788
UO_3	U	238.0	0.8322

2) **Conversion of atomic to weight abundance**

Atomic abundance gives the percentage of atoms of different isotopes in the natural sample. If the atomic abundance of i-th isotope is r_i, the average atomic weight is M_{av} and the atomic weight of the isotope is m_i then the weight abundance of this isotope will be

$$R_i = \frac{m_i}{M_{av}} \times r_i \qquad \text{(B.1)}$$

3) **Parent activity A_P in units of [Bq mg^{-1}] :**

$$A_P = \frac{\lambda \ N_A}{M} \times 10^{-3} \qquad \text{(B.2)}$$

where N_A is the Avogadro number (6.022 x 10^{23}), M is the atomic weight of the parent and λ is the decay constant ($\lambda = \ln 2/\tau_{1/2}$, $\tau_{1/2}$ is the half-life in seconds, 1 year = 31.56 x 10^6 s, 1 Bq=1 disintegration per second)

4) **Dose rate [Gy ka^{-1}] per ppm by weight of parent element**

$$\dot{D} = 5.056 \times A_P E_P \times 10^{-3} \qquad \text{(B.3)}$$

where E_P is energy release in the series per parent disintegration expressed in [MeV]. The numerical factor is based on 1 [MeV] = 1.602 x 10^{-13} [J]

5) **Dose rate in [Gy ka^{-1}] when parent activity is given:**

$$\dot{D} = 5.056 \times E_P c \times 10^{-3} \qquad \text{(B.4)}$$

where c is the specific activity of parent in the sample in [Bq kg^{-1}].

6) **Alpha count-rate when parent activity is given**

If C Bq kg^{-1} is the activity of parent, the thick-source alpha count-rate [ks^{-1}] is equal to

$$\dot{\alpha} = \frac{1}{4} fAR\rho \, nC \times 10^{-4} \qquad \text{(B.5)}$$

where f is the electronic threshold fraction, A cm^2 is the area of the scintillator, $R\rho$ is the average (projected) range expressed in [μg mm^{-2}], and n is the effective number of alpha emissions.

7) Effective alpha dose-rate

As explained in various sources, such as Aitken & Bowman (1975), Bowman & Huntley (1984) or Aitken (1985), the effective alpha dose-rate is given by

$$D' = 31.56 \times \eta\, bR'\rho\, nc \times 10^{-6} \qquad \text{(B.6)}$$

where η is the efficiency factor that makes allowance for the lower average energy of the natural spectrum experienced during burial compared to the particle energy used for measurement of alpha sensitivity (see note 5 of Table 7), b [Gy μm^2] is the dose of beta (or gamma) radiation required to induce the same luminescence, in the sample concerned, as an alpha track density of 1 [μm^{-2}], and $R'\rho$ is the average *total* range which is taken as $1.008 \times R\rho$ on the basis that the difference is approximately 0.4 [μg mm^{-2}] (Brennan & Lyons 1989).

Hence from (B.5), and changing to the a-value system by putting $b = 13a$,

$$D' = 16.54 \times \frac{\eta\, a}{fA} \times \alpha \qquad \text{(B.7)}$$

For measurement of either a or b it is necessary to have an alpha source calibrated in terms of track-length delivered and to have sufficient separation between source and sample that appreciably oblique particles are avoided; both source and sample must be in vacuum; the energy of the incident particles needs to be in the range 4-6 MeV and the layer of sample needs to be thin enough for emergent particles to have an energy of not less than 2 MeV.

References

Aitken M. J. (1974) *Physics and Archaeology.* Clarendon Press, Oxford.

Aitken, M.J. (1985) *Thermoluminescence Dating.* Academic Press, London.

Aitken, M.J. (1998) *Introduction to Optical Dating.* Oxford University Press.

Aitken M. J. & Bowman S. G. E. (1975) Thermoluminescent dating: assessment of alpha particle contribution. *Archaeometry* **18**, 132-138.

Bell W. T. (1976) The assessment of the radiation dose-rate for thermoluminescence dating. *Archaeometry* **18**, 107-110.

Bell W. T. (1977) Thermoluminescence dating: revised dose-rate data. *Archaeometry* **19**, 99.

Bell W. T. (1979) Thermoluminescence dating: radiation dose-rate data. *Archaeometry* **21**, 243-246.

Bowman S. G. E. (1976) Thermoluminescent dating: the evaluation of radiation dosage. Unpublished D.Phil. thesis, Faculty of Physical Sciences, Oxford University.

Bowman S. G. E. & Huntley D. J. (1984) A new proposal for the expression of alpha efficiency in TL dating. *Ancient TL* **2**, 6-11.

Brennan B. J. & Lyons R. G. (1989) Ranges of alpha particles in various media. *Ancient TL* **7**, 32-37.

Burrows T. W. (1988) The Program RADLST. *Brookhaven National Report:* BNL-NCS-*52142*. Obtainable from the National Technical Information Service (NTIS), U.S. Department of Commerce, 5285 Port Royal Road, Springfield, VA, USA (Fax: + 1 703 321-8547).

Carriveau G. T. & Troka W. (1978) Annual dose-rate calculations for thermoluminescence dating. *Archaeophysica* **10**, 406-422.

ICRP-38 (1983) *Annals of the ICRP Vol. 11-13, Radionuclide transformations: energy and intensity of emissions.* Pergamon, Oxford.

Krbetschek M. R., Rieser U., Zöller L., & Heinicke J. (1994) Radioactive disequilibria in palaeodosimetric dating of sediments. *Radiation measurements* **23**, 4485--489.

Liritzis Y. & Kokkoris M. (1992) Revised dose-rate data for thermoluminescence/ESR dating. *Nuclear Geophysics* **6**, 423-443.

Lyons R. G. & Brennan B. J. (1989) Alpha dose rate calculations in speleothem calcite: values of η and k_{eff}/k_{ref}. *Ancient TL* **7**, 1-4.

Martin M. J. & Blichert-Toft P. H. (1970) Radioactive Atoms. Auger-Electron, α, β, γ and X-Ray Data. *Nuclear Data Tables* **A8**, 1- 198.

Nambi K. S. V. & Aitken M. J. (1986) Annual dose conversion factors for TL and ESR dating. *Archaeometry* **28**, 202--205.

Ogoh K., Ikeda S., & Ikeya M. (1993) *Advances in ESR Applications* **9**, 22-29.

Olley J. M., Murray A. S., & Roberts R. G. (1997) The effects of disequilibria in the uranium and thorium decay chains on burial dose rates in fluvial sediments. *Quaternary Science Reviews (Quaternary Geochronology)* **15**, 751-760.

Valladas G. & Valladas H. (1982) Effet de l'irradiation alpha sur des grains de quartz. *PACT* **6**, 171-178.

Valladas G. (1988) Stopping power and range for alpha particles in SiO_2. *Ancient TL* **6**, 7-8.

Woithe J. M. & Prescott J. R. (1995) "Efficiencies" of phosphor screens used in thick source alpha particle counting. *Ancient TL* **13**, 10-15.

Zeigler J. F. (1977) *Helium, stopping powers and ranges in all elemental matter.* Pergamon, Oxford.

Zeigler J. F., Biersack J. P., & Littmark U. (1985) *The stopping and range of ions in solids* Vol 1 (ed. Zeigler) Pergamon, New York.

Zimmerman D. W. (1971) Thermoluminescent dating using fine grains from pottery. *Archaeometry* **13**, 29-52.

Reviewer

K.S.V. Nambi

Dose determination on fossil tooth enamel using ESR spectrum deconvolution with Gaussian and Lorentzian peak shapes

Rainer Grün

Research School of Earth Sciences
Australian National University
Canberra ACT 0200
Australia

(Received 11 March 1998 ; in final form 01 June 1998)

Abstract. *ESR spectrum decomposition was carried out with the commercial PeakFit program using Gaussian and Lorentzian peak shapes. The results show that there is at least one component in the ESR spectrum that yields significantly lower dose values than the central peak region which is used for conventional peak-to-peak dose determinations. Both deconvolution methods yield closely similar results to simple plateaux dose assessments, which are presently much faster to perform.*

Introduction

Recent publications have shown that the central region around g=2 of ESR spectra of tooth enamel consists of a number of separate peaks (e.g. Jonas et al. 1994, Jonas & Grün 1997). Jonas (1997) concluded that probably all published dose values on enamel may be erroneous. He used a fitting program developed for mainframes which required extremely long calculation times. Fortunately, commercial programs do pretty much the same, although some restrictions such as constant peak ratios or line widening cannot be implemented. In this study, the program PeakFit v4.0 (AISN Software 1995, distributed by Jandel Scientific) was used, which applies the same fitting optimisation strategies as the Jonas program.

Jonas (1997) used Gaussian line shapes for spectrum deconvolution and observed four main peaks with the following parameters (g-value; line width): #1 (2.0023; 3.8 G); #2 (1.9995; 5.1 G); #3 (2.0068; 23.4 G) and #4 (2.0034; 12.1 G - note that all line widths here and in the tables are in 2-σ). Peaks #1 and #2 may constitute an axial peak which has been attributed to the CO_2^-- radical. In principle, this radical ought to have three principle g-values (see Table 1) and deconvolution of ESR spectra of powdered fossil tooth enamel using Lorentzian functions results in three distinctive peaks (Callens, pers. comm.).

Radical	g_x	g_y	g_z	line width (G)
CO_2^-	2.0033	1.9972	2.0021	4.8
CO_3^{3-}	2.0044	2.0033	2.0018	1.3
CO^-	2.0061	2.0033	2.0018	1.6

Table 1: *Line parameters for various radicals in hydroxyapatite (Callens et al. 1995)*

The rationale of this paper was to check whether spectrum deconvolution using Gaussian and Lorentzian peak shapes gives different results in dose estimation and whether these are different from peak-to-peak or plateau dose assessments. Fitting was applied on sample 1047 (a bovid tooth from Florisbad) for which extensive reproducibility tests have been carried out (Grün & Clapp 1996; Grün 1998). Forty powdered aliquots of a sample 1047 were irradiated in ten irradiation steps and each aliquot was measured ten times, resulting in 400 D_e estimations. The peak-to-peak dose value of this sample is 75.8±2.1 Gy, the rising dose plateau of the absorption spectrum ranges between 76.1±3.9 and 81.9±4.1 Gy and the dose value derived from the maximum of the absorption spectrum is 77.9±3.4 Gy. All of these results are statistically indistinguishable, but the somewhat higher dose values obtained from the absorption spectra (i.e. resulting form integration of a conventional derivative spectrum) was interpreted that some non-radiation sensitive peaks may interfere with the radiation sensitive.

The reason for using a fossil rather than an artificially

irradiated, recent sample lies in the fact that due to the long mean life of the signals involved, nearly all components of the irradiated sample will give the same, artificial dose. This may be useful for source calibration and inter-laboratory tests but cannot be used for identifying problems in the dose estimation of fossil samples (see also Grün 1998). Unfortunately, it is not possible to assess which dose value is correct on the basis of its independent assessment, because it is neither possible to date teeth precisely by independent means (radiocarbon dating is strongly influenced by rapid exchange of secondary carbonate; see Grün et al. 1997 and U-series dating is dependent on U-uptake; see Grün & McDermott 1994) nor to estimate the dose rate accurately (due to variations in water content in the sediment and dentine as well as uranium uptake in enamel and dentine).

Experimental

For details of experimental setup, measurement parameters and spectrum manipulation see Grün (1998). PeakFit runs on IBM compatible computers and a typical deconvolution calculation (once the peak parameters are defined) takes between 20 and 60 seconds on a PC with a 150 MHz Pentium processor. In this study, I used the averaged spectra from the ten repeated measurements of each dose step of the first aliquot. Firstly, the ten averaged ESR spectra of the ten dose steps were integrated (without baseline corrections), aligned on the maximum intensity and normalised on maximum peak intensity. This ensured that the influence of each spectrum on the averaged spectrum was more or less the same. Then the spectra were added and averaged. This averaged spectrum was used for deconvolution and estimation of the peak parameters. Peak width and position were then locked for the fitting of the individual spectra representing the different dose steps. Gaussian curves are described by:

$$\text{ESR Intensity} = \text{Amplitude} \exp(-0.5\ (\text{Magnetic Field} - \text{Line Centre})/1\text{-}\sigma\ \text{Line Width})^2)$$

and Lorentzian by:

$$\text{ESR Intensity} = \text{Amplitude} / (1 + (\text{Magnetic Field} - \text{Line Centre})/1\text{-}\ \sigma\ \text{Line Width})^2)$$

The differences between Gaussian and Lorentzian line shapes are relatively small, Lorentzian peaks have longer tail ends (see Figure 1). Figure 1A shows the derivative averaged ESR spectrum of sample 1047. It is dominated by an apparently axial peak which has been attributed to CO_2^- (e.g. Callens et al. 1995). The quintet which is centred on the top of the large central signal at g = 2.0032 (*) has been attributed to alanine (Ikeya 1982) or a dimethyl radical (Bouchez et al. 1988), the line at g=2.0056 (+) may be due to CO^- (see Fig. 3b of Callens et al. 1995) or a free radical (Bouchez et al. 1988) which could be SO_2^- (Barabas 1992, Ikeya 1993). The isotropic line at g = 2.0114 (#) is a rotating CO_3^--radical (Moens et al. 1993).

Results and discussion

Following the experiments of Jonas (1997), the ESR spectra were firstly deconvoluted using 4 Gaussian and 4 Lorentzian peaks. For a reasonable fit of the Lorentzian peaks it was necessary to introduce a further line at high magnetic fields (L5). The resulting parameters are shown in Table 1 and Figures 1B and 1C.

The g-values were calculated by using a DPPH standard. There seems to be an offset of 0.0005 between these values and those of Jonas (1997) who used a Mn^{2+} standard. The Gaussian lines attributed to CO_2^- (#1 and #2 of Jonas and lines G3 and G4 in this study) agree fairly well whilst the other two lines have considerably different line widths and central positions. However, this is not surprising, because Jonas (1997) used scans over about 80 G whereas this study uses 120 G wide scans.

As can be seen in Figure 1B-D, the integrated spectrum shows already significant ESR-intensity at ± 40 G around the main peak. Thus, the deconvolution results in the much wider line G2. Both studies have in common that the central peak is represented by two Gaussian peaks (which may combine into an axial line shape) which are overlapped by two wider lines. The three Lorentzian lines representing the central peak are only interfered by one other line.

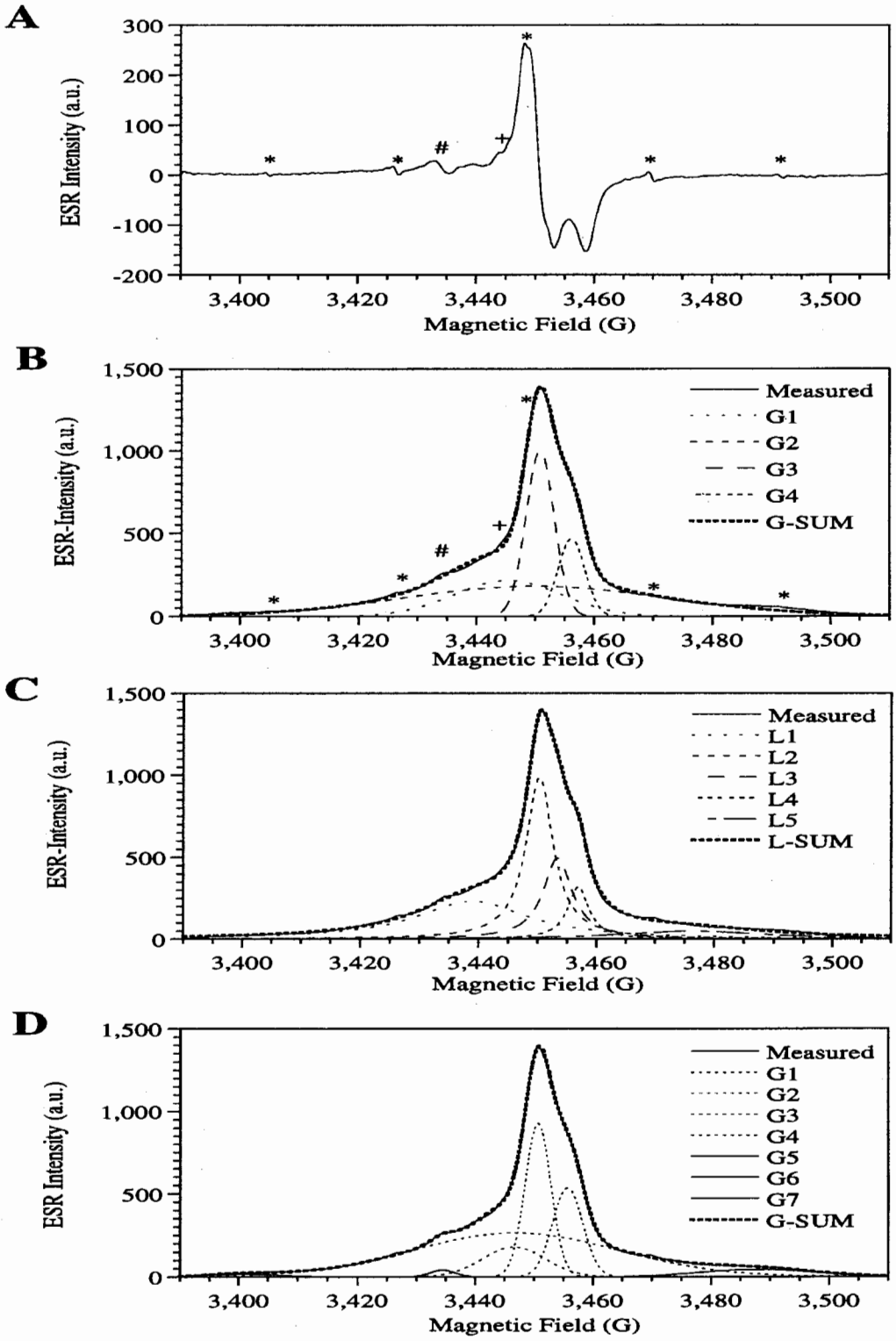

Figure 1

A: Averaged derivative spectrum of sample 1047. It is dominated by an apparently axial peak which has been attributed to CO_2^- . The quintet which is centred on the top of the large central signal at g = 2.0032 (*) has been attributed to alanine or a dimethyl radical; the line at g=2.0056 (+) may be due to CO^- or a free radical which could be SO_2^-. The isotropic line at g = 2.0114 (#) is a rotating CO_3^--radical.

B: Fitting of the integrated spectrum with 4 Gaussian peaks, for peak parameters see Table 2.

C: Fitting of the integrated spectrum with five Lorentzian peaks.

D: Fitting of the integrated spectrum with seven Gaussian peaks.

It can be seen that the ESR spectrum is not 100% fitted by the four Gaussian lines, particularly around 3333 G, the location of the isotropic CO_3^-- radical (#) and at 3490 G. Therefore, a second Gaussian deconvolution experiment was carried out, using seven peaks (r^2 = .9998). As can be seen in Figure 1D, the two central peaks (G3: g=2.0019; width: 4.4 G and G4: g=1.9990; width: 5.1G) change little, but the position, width and relative intensity of G1 (g=2.0043; width: 10.6 G) and G2 (g=2.0041; width 35 G) change substantially
Using the integrated areas of the four and seven Gaussian and five Lorentzian lines, the dose values given in Table 3 were obtained.

The fitting of the ESR spectra with Gaussian line shapes with either 4 or 7 peaks yielded more robust results than the Lorentzian line shapes and were accompanied with better correlation coefficients. This may be an indication that Lorentzian peak shapes are not as appropriate for this sample as the Gaussian. The dose response of the total integral yields 88±10 Gy and its fitting is considerably worse than the fitting of any of the above components.

All three experiments have in common that the first line (G1 and L1), which strongly interferes with G3, yields significantly lower dose values than the central peaks. The wide line G2 yields the same dose value as the central peak region. Furthermore, those lines which are less influenced by the first line (G4, L4) give somewhat higher dose values than G3 or L2, L3. This may be taken as indication that the different components are not completely separated by the deconvolution process. On the other hand, the derivative spectrum shows various interferences of the central peak region (see Figure 1A) which are not resolved in the integrated spectrum. These peaks may well influence the dose value of G3 and L2, L3.

The dose values derived from the central peak region (G3&4, L2-4) are all slightly higher than the peak-to-peak dose value of the derivative spectra of 75.8±2.1 G. The dose results of G3 and G4 agree very well with the two ends of the "rising plateau" observed by Grün (1998) which yielded dose values of 76.1±3.9 in the region of G3 and 81.9±4.1 Gy in the region of G4. Considering the effect of G1 on G3, the most realistic dose value ought to derive from G4 (around 82 Gy) which is about 8% higher than the conventional peak-to-peak dose value. The dose response curve of L5 shows by far the largest scatter of the data points (it is also the smallest peak) and the L5 dose value is probably not too significant.

Similarly to the experiments of Jonas (1997), it not possible to relate the Gaussian and Lorentzian peaks directly to components of the CO_2^- or CO_3^--radicals. The line widths of G3 and G4 indicate a relationship with the CO_2^- radical whereas G1 may represent the whole CO_3^--radical. Clearly, the best solution for realistic dose assessment lies in the fitting of physically meaningful line shapes to the ESR spectra. However, so far the dose response curves of such deconvolution methods have yielded dose response curves which contain significantly more scatter than any of the methods discussed in this paper (Callens, pers. comm.).

	Gaussian peaks				Lorentzian peaks			
No	Position (G)	g-value	Width (G)	Amplitude	Position (G)	g-value	Width (G)	Amplitude
1	3445.4	2.0050	18.0	216	3439.0	2.0087	22.6	231
2	3449.9	2.0024	44.4	181	3450.4	2.0021	5.6	977
3	3450.9	2.0018	4.8	998	3453.4	2.0004	6.0	494
4	3456.2	1.9987	4.6	466	3457.0	1.9983	4.4	318
5					3476.2	1.9872	29.0	48
r^2		0.9988				0.9983		

Table 2: *Results of spectrum deconvolution of the averaged spectrum of sample 1047 (see Figure 1). The labelling is simply sequential and should not be used to infer any relationship between the Gaussian and Lorentzian peaks.*

It is clear that extensive calculation times on main-frames are not required for adequate spectrum deconvolution using Gaussian or Lorentzian line shapes. The time for routine spectrum preparation, deconvolution and fitting may be in the range of one hour per sample. This compares to one to two minutes for plateau fitting. Considering that the plateau dose values are closely similar to those of deconvolution (at least in this case), it seems most economical to calculate plateaux first and invoke deconvolution as check and on selected sets which indicate stronger interferences of the central peak region (see e.g. Grün & Jonas 1996)

No	4 Gaussian peaks Dose (Gy)		Lorentzian peaks Dose (Gy)		7 Gaussian peaks Dose (Gy)
1	40.2±1.6		37.4±5.9		41.5±4.1
2	78±45		78.7±2.2		75±15
3	78.7±2.1		73.1±3.4		75.3±2.6
4	82.7±1.9		114±11		82.2±2.5
G3&4	80.3±2.0	L2-4	82.5±5.0	G3&4	77.6±2.5

Table 3. *Dose results*

References

Barabas, M. (1992) The nature of the paramagnetic centres at g = 2.0057 and g = 2.0031 in marine carbonates. Nuclear Tracks and Radiation Measurements **20(3)**: 453-464.

Bouchez, R., Cox, R., Herve, A., Lopez-Carranza, E., Ma, J.L., Piboule, M., Poupeau, G. and Rey, P. (1988) Q-band ESR studies of fossil teeth, consequences for ESR dating. Quaternary Science Reviews **7**: 497-501.

Callens, F., Moens, P. and Verbeeck, R. (1995) An EPR study of intact and powdered human tooth enamel dried at 400°C. Calcified Tissues International **56**:543-548.

Grün, R. (1998) Reproducibility measurements for ESR signal intensity and dose determination: high precision but doubtful accuracy. Radiation Measurements **29** : 177-193.

Grün, R., Abeyratne, M., Head, J., Tuniz, C. and Hedges, R.E.M. (1997a) AMS ^{14}C analysis of teeth from archaeological sites showing anomalous ESR dating results. Quaternary Geochronology (QSR) **16**: 437-444.

Grün, R. and Clapp, R. (1996) An automated sample changer for Bruker ESR spectrometers. Ancient TL **14**: 1-5.

Grün, R. & Jonas, M. (1996) Plateau tests and spectrum de-convolution for ESR dose determination. Radiation Measurements **26**: 621-629.

Grün, R. & McDermott, F. (1994) Open system modelling for U-series and ESR dating of teeth. Quaternary Geochronology (QSR) **13**: 121-125.

Ikeya, M. (1982). A model of linear uranium accumulation for ESR age of Heidelberg, Mauer, and Tautavel bones. Japanese Journal of Applied Physics **21**: L690-L692.

Ikeya, M. (1993). *New Applications of Electron Spin Resonance - Dating, Dosimetry and Microscopy*. Singapore, New Jersey, London, Hong Kong, World Scientific.

Jonas, M. (1997) Electron spin Resonance dating and dosimetry of tooth enamel. Unpublished PhD Thesis, University of Cambridge.

Jonas, M. and Grün, R. (1997) Q-band ESR studies of fossil tooth enamel: implications for spectrum deconvolution and dating. Radiation Measurements **27**: 49-58.

Jonas, M., Zhou, L.P., Marseglia, E. and Mellars, P. (1994) New analysis of ESR spectra of fossil tooth enamel. Cambridge Archaeological Journal **4**: 139-146.

Moens, P., De Volder, P., Hoogewijs, R., Callens, F. & Verbeek, R. (1993) Maximum-likelihood common-factor analysis as a powerful tool in decomposing multicomponent EPR powder spectra. Journal of Magnetic Resonance **A101**:1-15.

Reviewer

Henry Schwarcz

An assessment of the Levenberg-Marquardt fitting algorithm on saturating exponential data sets.

Robert B. Hayes, Edwin H. Haskell and Gerry H. Kenner

University of Utah ,Radiobiology Div.. Center for Applied Dosimetry
729 Arapeen Dr. SLC, UT 84108-1218, U.S.A
email; r.b.hayes@m.cc.utah.edu . Phone; 801-585-4018

(Received 17 June 1998 ; in final form 20 October 1998)

Introduction

A common, flexible curve fitting algorithm has recently become available in a commercial graphical software package for both PC's and Mac's (Kaleidagraph©). The source code of the algorithm is also available from standard numerical recipes packages in FORTRAN, BASIC, Pascal and C (©Press et al. 1992). We assess the algorithm's ability to model saturating dose responses by comparing it to other established methods using the test data of Berger and Huntley (1989) for two intersecting and saturating curves constructed from the partial bleach method. The utility of the package for other applications is also discussed.

The Levenberg-Marquardt (LM) algorithm has some unique properties relative to other, more established algorithms devoted to modeling saturating exponential data sets (Berger et al. 1987, Brumby 1992, Grün and Macdonald 1989, Poljakov and Hütt 1990). It has been validated as an excellent tool for deconvoluting EPR spectra (Haskell et al. 1996A&B, Haskell et al. 1997A&B, Kenner et al. 1998, Jonas 1995 & 1997, Pilawa et al. 1995, Polyakov et al. 1995) and has also been used for, or in conjunction with, TL spectral deconvolution (Lucas and Akselrod 1996, Emfietzoglou and Moscovitch 1996). The algorithm can also fit standard OSL curves containing multiple centers scanned using either the conventional shine down method or the new linear modulation technique (Bulur 1996, Bulur and Göksu 1997, Figure 1). This allows the same software to be used for multiple applications, from first determining the measurement amplitude (via deconvolution) to fitting the resultant dose response.

The form of this dose response can vary from a linear response to multiple saturating exponentials (and virtually all other forms including sublinear, supralinear etc.) while still being modeled appropriately with the algorithm (assuming that the correct model is used). The algorithm also provides uncertainty estimates for all parameters of the fit. A tangential application where this becomes useful is in estimating the saturation dose for the material being studied. This is required to determine when a linear fit rather than a saturating exponential fit should be applied to the data (i.e., the maximum dose applied should be $\leq 1\%$ of the saturation dose for linear fitting to be statistically more accurate, see Grün 1996). However, this criterion should only be applied if accurate values with reliable uncertainties can be assured. The importance of using the correct model, errors and fitting procedure is clearly laid out in the literature (Berger et al. 1987, Berger 1990, Grün 1996, Grün and Brumby 1994, Grün and Rhodes 1992, Grün and Packman 1993, Guibert et al. 1996, Lyons et al. 1992).

The LM method for nonlinear fitting is a numerical compromise between the Gauss-Newton method of linearization (used by Berger et al. 1987) and that of steepest descent. The LM method uses a least squares criterion for convergence and can therefore be expected to give results similar to the method of Poljakov and Hütt (1990) (which iteratively uses a strict least squares method to determine two parameters and a Newton-Raphson method to determine the third) for unweighted saturating exponential data. In generating the curve parameters, the LM algorithm also generates the covariance matrix for the model and data (see Press et al. 1992). It is from the diagonals of the covariance matrix that the individual variances of the fitted parameters are taken (Press et al. 1992). The LM method does require that the initial estimates be sufficiently near (typically within an order of magnitude, Motulsky 1997) the optimum values to attain a reliable convergence.

Aliquot curve parameter	GWB	S C	S-m	DOSE	LM
QNL84-2 unbleached I_0 (x 10^{-4})	14.28	14.25 ± 0.46	14.25	-	14.25 ± 0.56
QNL84-2 unbleached D_x	122.7 ± 6.7	121.9 ± 6.7	121.9	121.9 ± 6.8	122.0 ± 8.3
QNL84-2 unbleached D_0	392	390 ± 31	389.9	-	390 ± 38
QNL84-2 bleached I_0 (x 10^{-4})	9.64	9.7 ± 1.0	9.67	-	9.67 ± 0.86
QNL84-2 bleached D_x	193 ± 19	195 ± 20	195.2	195 ± 20	195 ± 17
QNL84-2 bleached D_0	762	770 ± 150	773	-	770 ± 130
STRB87-1 unbleached I_0 (x 10^{-4})	21.21	21.15 ± 0.48	21.15	-	21.18 ± 0.45
STRB87-1 unbleached D_x	0.583 ± 0.018	0.583 ± 0.018	0.583	0.591 ± .020	0.591 ± 0.017
STRB87-1 unbleached D_0	5.96	5.95 ± 0.25	5.95	-	5.98 ± 0.23
STRB87-1 bleached I_0 (x 10^{-4})	12.043	12.03 ± 0.32	12.03	-	12.03 ± 0.32
STRB87-1 bleached D_x	0.680 ± 0.023	0.682 ± 0.023	0.682	0.682 ± 0.023	0.682 ± 0.023
STRB87-1 bleached D_0	6.67	6.68 ± 0.31	6.68	-	6.68 ± 0.31
STRB87-1 intersection	0.485 ± 0.037	0.481 ± 0.080	-	-	0.481 ± 0.031
QNL84-2 intersection	86 ± 10	85 ± 21	-	-	85 ± 28

Table 1.
Curve parameters from modeling saturating exponential data. Corresponding error estimates (when available) are also given. Here I_0 is the saturation intensity, D_x is the dose estimate and D_0 is the characteristic saturation dose. The GWB method is the quasi-likelihood method of Berger et al. (1987), SC is the simplex algorithm (Berger and Huntley 1989), S-m is a weighted least squares method (Berger and Huntley 1989), DOSE is the simplex algorithm with quadratic convergence from Brumby (1992) and LM is the Levenberg-Marquardt method. The error estimators of the two curve intersections for the LM method were calculated using basic first order error propagation.

Like the methods of Brumby (1992), Grün and Macdonald (1989) or Poljakov and Hütt (1990), the LM fitting method does not have the ability to rigorously assess the relative error distribution of the data as does that of Berger et al. (1987). These errors must be independently determined if LM fitting is to be used (a very basic and simple method for estimating these uncertainties is described below). This is important because Grün and Rhodes (1992) verified the earlier derivation of Berger et al. (1987, appendix A) that curve fits to saturating exponential dosimetry data should be weighted by relative terms. It should be pointed out, however, that if a case were found where relative errors could be demonstrated to be negligible, then this would no longer be expected to be the case and equal weighting would be expected to give better results (Franklin 1986). The most common instance in which this will occur is when the high frequency noise from the measurement instrumentation (or other source) becomes large relative to the size of the dosimetric signals being evaluated. Examples fulfilling this criterion, and more precise descriptions of the effect, are given both by Hayes et al. (1997) and Scott and Sanderson (1988). In general, this is not expected to be observed in geological dating studies but should be restricted to more recent archeological dose reconstructions (Grün and Macdonald 1989). When the case of mixed errors is encountered (where neither the constant or relative errors are negligible), the appropriate weighting terms are given by Bluszcz (1988).

Using the saturating exponential test data of Berger and Huntley (1989), with the modified data point mentioned by Huntley (1996), we compare the results of the LM routine to the quasi-likelihood method of Berger et al. (1987), the simplex method (Berger and Huntley 1989), a weighted least squares method (Berger and Huntley 1989) and the quadratic convergance method of Brumby (1992).

Results

The LM method appears to be comparable in both parameter and error estimation to the other fitting methods based on the results given in Table 1 (error estimates were not available for all the parameters of some of the other fitting methods). Here, we have included the calculations of the intersections and the first order error estimates of the uncertainties associated with the two intersections. The data were weighted with either 4% or 3% relative errors as done in Berger and Huntley (1989) so that a direct comparison could be made to their data. This was done because the calculated errors (not the fitted parameters) using the LM fitting method for data weighted by inverse variance are directly proportional to the relative error selected (which is true for other methods also). If the weights chosen were increased or decreased by a factor of ten, then the error estimates would also be increased or decreased by a factor of ten respectively despite the identical fitted parameter values.

Because of the necessity to weight saturating data by relative errors, the magnitude of the relative error must be reasonably estimated and supplied to the LM algorithm prior to the fit. We offer a simple, model-dependent method. This is to initially fit the data with a weighted saturating exponential (here the weights are relative errors of arbitrary magnitude) to first estimate the residuals (the residual for each data point is the vertical distance from that point to the curve fit). We then divide each residual by the magnitude of the curve fit at the respective point. After taking the average of these numbers, we can equate this to the relative error magnitude which we should use in the LM method for a weighted fit to the data. This approach assumes both a correct model was employed in the weighted fit (e.g., single saturating exponential) and that the residuals are Gaussian distributed with variance dominated by relative values (constant errors, systematic errors etc. are assumed negligible). Because the fitting parameters will not be affected by a change in the magnitude of the weighting terms of the relative error (only their error estimators will be), iteration is not necessary for this approach. Application of this method resulted in average relative error amounts of 2.2% for the STRB87-1 measurements and 2.9% for the QNL84-2 measurements.

It should be pointed out that this simple approximation method is not offered as an optimal approach but rather as an easy to use approximation. It will not be acceptable in all cases. Indeed the main advantages of other established methods (Berger et al. 1987) over that of LM is their implicit ability to determine the respective weights for use in fitting each data set and to iteratively assess the uncertainty in the intersection of the two curve fits.

Some comments addressing convergence reliability and accuracy are now in order. Our comments are based on 4 years experience of modeling dose response data using the LM algorithm. When the maximum dose is less than about 10 percent of the saturation dose (D_O,) the estimates and associated uncertainties for both D_O and the saturation intensity I_O will converge to arbitrarily large values (with the uncertainties being typically at least a few orders of magnitude larger than their associated parameters). In the same situation however, the x-intercept of the fit with its estimated uncertainty is similar to that obtained using a linear fit. The algorithm otherwise will converge (with reasonable parameter and uncertainty

estimates) for all data sets even when the relative errors are approaching 30% (which indicates the data set itself is not useful).

Example

A straightforward application for LM deconvolution is shown in Figure 1 which was done entirely using the software package Kaliedagraph©. Here we show a spectrum from the dose response of a K-feldspar sample. The sample was scanned using the new linear modulation method of OSL (Bulur 1996). The resultant dose response from the three signals used to model the spectrum are shown in Figure 2. The data for Figures 1 and 2 were supplied by Enver Bulur.

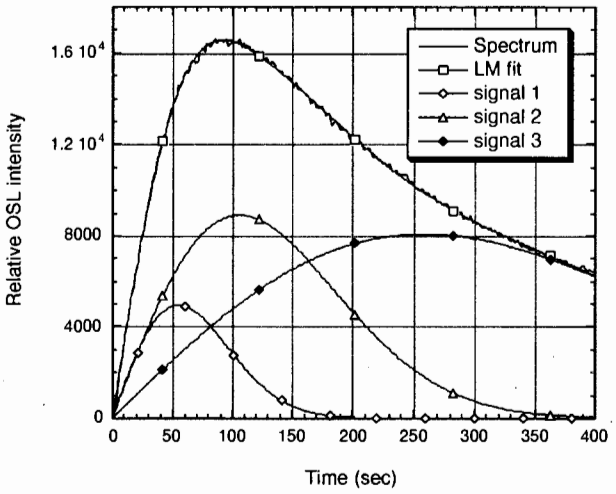

Figure 1.

Spectral deconvolution of an OSL curve recorded using the linear modulation technique (Bulur 1996). The curve fits used an unweighted model. This spectrum was chosen for the figure because it had the lowest correlation (it also had the lowest dose of 2.825 Gy) . The form of the curve used for the model assumed first order kinetics resulting in curve shapes of the form

$$Y=-m1*X*\exp(-X^2/(2*m2^2))/\ m2^2.$$

This allowed us to consider only the dependence on the m1 parameter for the dose response although the m2 parameter was consistently stable to within 2% for each signal.

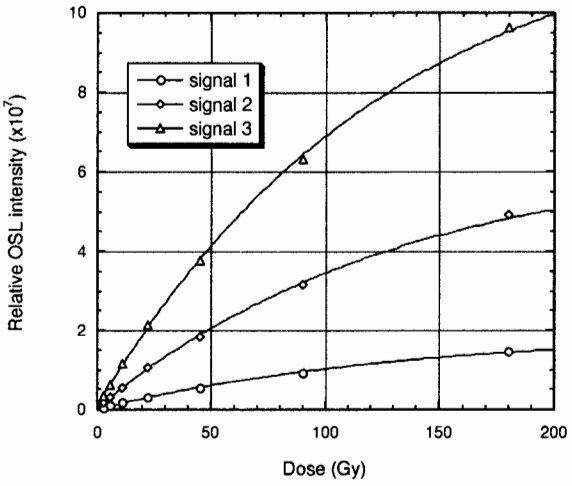

Figure 2.

Curve fit to the saturating exponential data set generated by the linear modulation OSL technique. The curve fit for each dose response from the three deconvoluted signals shown in Figure 1 are displayed. By plotting the m1 parameter (see caption to Figure 1) we effectively plot the integrated spectrum of each signal. Using the method described in the text for the LM algorithm, the fits were weighted with 2% relative errors. The applied doses were 2.825, 5.625, 11.25, 22.5, 45, 90 and 180 Gy. This resulted in reconstructed doses D_X of 420±95 mGy, 424±28 mGy and 686±106 mGy for signals 1, 2 and 3 respectively.

Conclusion

Because it is available as either a canned numerical routine (Press et al. 1992) or an integrated component of a commercial graphing software package (Kaleidagraph©), the LM fitting routine is readily available with little required effort of the user. Reasonable estimates may now be obtained in a user friendly graphing program using a viable algorithm for modeling many of the data sets encountered in dating and retrospective dosimetry.

It should be born in mind however that for the specific application considered here (determination of the intersection of two intersecting saturating exponentials), more accurate and precise algorithms can be found in the literature (Berger et al. 1987). This is due to both the lack of the LM algorithm to do any implicit and rigorous treatment of the dual curve intersection error analysis and also its inability to implicitly determine the error distribution of the data set it is modeling.

The method has some potential benefits not offered by certain other routines in use. In particular, it has the necessary flexibility to model saturating-exponential-plus-linear data (Hütt and Smirnov 1983, Berger 1990, Berger 1991), multiple

saturating exponentials (Katzenberger and Willems 1988, Packman and Grün 1992), data with supralinearities (Valladas and Gillot 1978) or any number of other models used in TL/EPR dose responses (Berger 1985, Berger 1987, Guibert et al. 1996). The minimum requirements for using the algorithm is that both the fitting function and its gradient can be calculated (if these are not given in closed form then numerical calculation can be implemented at the cost of convergence speed).

Acknowledgments

We would like to thank Dr. Enver Bulur for graciously providing us with data he recorded using the linear modulation OSL technique. This work supported by the U.S. Department of Energy, Contract DE-FC03-97SF1354.

References

Berger G. W. (1985) Thermoluminescence dating applied to a thin winter varve of the Late Glacial Thompson Silt, south-central British Columbia. *Can. J. Earth Sci.*, **22**, 1736-1739.

Berger G. W. (1987) Thermoluminescence dating of the Pliestocene Old Crow tephra and adjacent loess, near Fairbanks, Alaska. *Can. J. Earth Sci.*, **24**, 1975-1984.

Berger G. W. (1990) Regression and error analysis for a saturating-exponential-plus-linear model. *Ancient TL*, **8**, 23-25.

Berger G. W. (1991) The use of glass for dating volcanic ash by thermoluminescence. *J. Geophys. Res.*, **96**, 19705-19720.

Berger G. W. and Huntley D. J. (1989) Test data for exponential fits. *Ancient TL*, **7**, 43-46.

Berger G. W., Lockhart R. A. and Kuo J. (1987) Regression and error analysis applied to the dose-response curves in thermoluminescence dating. *Nucl. Tracks Radiat. Meas.*, **13**, 177-184.

Bluszcz A (1988) The Monte-Carlo experiment with the least squares methods of line fitting. *Nucl. Tracks Radiat. Meas.* **14**, 355-360.

Brumby S. (1992) Regression analysis of ESR/TL dose-response data. *Nucl. Tracks Radiat. Meas.*, **20**, 595-599.

Bulur E. (1996) An alternative technique for optically stimulated luminescence (OSL) experiment *Radiat. Meas.* **26**, 701- 709.

Bulur E. and Göksu H. Y. (1997) IR stimulated luminescence from ZnS and SrS based storage phosphors: a re-examination with linear modulation technique. *Phys. Stat. Sol. (Rapid Research Notes)* **161**, R9-R10.

Emfietzoglou D. and Moscovitch M.. (1996) Phenomenological study of light-induced effects in a-Al_2O_3:C. *Radiat. Prot. Dos.*, **65**, 259-262.

Grün R. (1996) Errors in dose assessment introduced by the use of the "linear part" of a saturating dose response curve. *Radiat. Meas.*, **26**, 297-302.

Grün R. and Brumby S. (1994) The assessment of errors in past radiation doses extrapolated from ESR/TL dose-response data. *Radiat. Meas.*, **23**, 307-315.

Grün R. and Macdonald P. D. M. (1989) Non-linear fitting of TL/ESR dose-response curves. *Appl. Radiat. Isot.*, **40**, 1077-1080.

Grün R. and Packman S. C. (1993) Uncertainties involved in the measurement of TL intensities. *Ancient TL*, **11**, 14-20.

Grün R. and Rhodes E. J. (1992) Simulation of saturating exponential ESR/TL dose response curves - weighting of intensity values by inverse variance. *Ancient TL*, **10**, 50-56.

Guibert P., Vartanian E., Bechtel F. and Schvoerer M. (1996) Non linear approach of TL response to dose: polynomial approximation. *Ancient TL*, **14**, 7-14.

Haskell E., Kenner G., Hayes R., Chumak V. and Sholom S. (1996A) EPR dosimetry of teeth in past and future accidents: a prospective look at a retrospective method. *Effects of Low-Level Radiation for Residents Near Semipalatinsk Nuclear Test Site. Proceedings of the Second Hiroshima International Symposium.* M. Hoshi, J. Takada, R. Kim and Y. Nitta (Ed.). Research Institute for Radiation Biology and Medicine, Hiroshima University (Pub.). Hiroshima, Japan. 261-274.

Haskell E. H., Hayes R. B. and Kenner G. H. (1996B) Plasterboard as an emergency EPR dosimeter. *Health Phys.* **71**, 95.

Haskell E. H., Hayes R. B., Kenner G. H., Sholom S. V. and Chumak V. V. (1997A) EPR techniques and space biodosimetry. *Radiat. Res.* **148**, S51-S59.

Haskell E. H., Hayes R. B. and Kenner G. H. (1997B) Improved accuracy in EPR dosimetry using a constant rotation goniometer. *Radiat. Meas.* **27**, 325-329.

Hayes R. B., Haskell E. H. and Kenner G. H. (1997) A mathematical approach to optimal selection of dose values in the additive dose method of EPR dosimetry. *Radiat. Meas.*, **27**, 315-323.

Huntley D. J. (1996) Errata (Letters). *Ancient TL*, **14**, 31.

Hütt G. and Smirnov A. (1983) Thermoluminescence dating of sediments by means of the quartz and feldspar inclusion methods. *PACT*, **9**, 463-471.

Jonas M. (1995) Spectral deconvolution of the ESR dating signal in fossil tooth enamel. *Quat. Sci. Rev.*, **14**, 431-438.

Jonas M. (1997) *Electron Spin Resonance Dating of Tooth Enamel.* Ph.D. thesis, Cambridge University, Cambridge UK.

Katzenberger O. and Willems N. (1988) Interferences encountered in the determination of AD of mollusc samples. *Quat. Sci. Rev.*, **7**, 485-489.

Kenner G. H., Haskell E. H., Hayes R. B., Baig A. and Higuchi W. I., (1998) EPR properties of synthetic apatites, deorganified dentin and enamel. *Calcif. Tiss. Int.*, **62**, 443-446.

Lucas A. C. and Akselrod M. S. (1996) The determination of dose as a function of depth by deconvolution of the glow curve using thick TL dosimeters. *Radiat. Prot. Dosim.*, **66**, 57-62.

Lyons R. G., Brennan B. J. and Hosking P. L. (1992) Estimation of accumulated dose and its uncertainties: potential pitfalls in curve fitting. *Ancient TL*, **10**, 42-49.

Motulsky H. (1997) Fitting curves with nonlinear regression. *Scitech J.*, **7**, 20-23.

Pilawa B., Weickowski A. B. and Trzebicka B. (1995) Numerical analysis of EPR spectra of coal, trace macerals and extraction products. *Radiat. Phys. Chem.*, **45**, 899-908.

Packman S. C. and Grün R. (1992) TL analysis of loess samples from Achenheim. *Quat. Sci. Rev.*, **11**, 103-107.

Polyakov V., Haskell E., Kenner G., Huett G. and Hayes R. (1995) Effect of mechanically induced background signal on EPR dosimetry of tooth enamel. *Radiat. Meas.* **24**, 249-254.

Poljakov V. and Hütt G., (1990) Regression analysis of exponential palaeodose growth curves. *Ancient TL*, **8**, 1-2.

Press W. H., Teukolsky S. A., Vetterling W. T. and Flannery B. P. (1992) *Numerical Recipes in FORTRAN - The art of Scientific Computing. 2nd edn.* Cambridge University Press, New York. pp. 675-694.

Scott E. M. and Sanderson D. C. W. (1988) Statistics and the additive dose method in TL dating. *Nucl. Tracks. Radiat. Meas.*, **14**, 345-354.

Valladas G. and Gillot P. Y. (1978) Dating of the Olby lava flow using heated quartz pebbles. *PACT*, **2**, 141-150.

Reviewer
G. Berger

Comments
The authors deserve thanks for enduring my suggested iterative revisions. It is worth mentioning a few points here. All users of statistical packages should be alert to the assumptions and limitations of the methods used . The authors carefully point out that the LM method can be weak in error analysis (second last paragraph in Results section). Its strength appears to be in versatility and ease of use. Note that the « saturating exponential » model of Berger et al. (1987) can also be used successfully with most sublinear data, sometimes with supralinear data. However, as discussed by Berger et al. (1987), second-order polynomials (quadratics) may work better (as good approximation) than their exponential-model method for supralinear data, certainly for two intersecting curves. As well, the methods of Berger et al. (1987) and Berger (1990) probably may also be used to obtain estimates of uncertainties in certain fitting parameters (e.g. D_0 and I_0), but have not yet bothered to extract this information from the covariance matrices. Also, it appears that the authors' approximate method for estimating relative errors in advance of solution by LM is equivalent to the use of equation 4 in Berger et al. (1987), except that the latter includes a weighting term in this equation (making it iterative).

Finally, for new workers in TL/OSL/ESR it is worth mentioning that the basic arguments for the use of weighting by inverse variance have deep historical roots. Several of these roots are cited in Berger et al. (1987). Among these are citations of Deming (1949), and the papers of York. I urge readers to consult York's papers on regression and error analysis from time to time. Although his papers deal with linear models, some of the concepts are still relevant to sublinear models.

Improvements in infra-red dating of partially bleached sediments – the 'Differential' Partial Bleach Technique

A.K. Singhvi[1] and A. Lang[2]

[1]Earth Science Division, Physical Research Laboratory, Ahmedabad 380 009, India
[2]Forschungsstelle Archäometrie, Heidelberger Akademie der Wissenschaften, Max-Planck-Institut für Kernphysik, Postfach 103980, D-69029 Heidelberg, Germany

(Received 15 April 1998 ; in final form 9 October 1998)

Abstract *- A new approach to estimate optical ages making use of the most light sensitive component of partially bleached sediments is proposed. A differential partial bleach technique is used where the stimulation during measurement substitutes for the laboratory bleach. Results on infrared stimulated luminescence from fine grain sediments of diverse depositional environments, based on this approach are presented. Improvements are obtained in the case of poorly bleached sediments, whereas results for well bleached sediments are consistent with other optical dating results. The differential partial bleach technique is seen as primarily applicable to silt-sized sediments, for which single-grain dating is not feasible.*

Introduction

During the past few years a considerable effort has been expended towards developing methodologies for luminescence dating of fluvial, glacio-fluvial and colluvial sediments (see e.g. Berger, 1988, 1990). In contrast to aeolian deposits such sediments receive a substantially reduced daylight flux and a narrower spectrum for photobleaching prior to deposition. This is due to a combination of sediment load, turbulence in the medium and clumping of sediment particles. In such sediments there are three possible scenarios of pre-depositional daylight exposure, viz.,

(1) that all grains experienced equal but a substantially attenuated bleaching,
(2) that the grains were bleached to varying extent,
(3) a combination of the above, i.e. the grains were both poorly and heterogeneously bleached.

To address to the problem of uniform insufficient bleaching (#1 above), the partial bleach TL method was developed. This was based on an assumption that the luminescence level of a mineral grain comprises several components with different sensitivity to photobleaching (Wintle and Huntley, 1979, 1980; Huntley, 1985). Thus in a uniformly but partially bleached sediment with a complex history of depositional photobleaching it is expected that only a part of the signal was bleached and the other part was not affected. It is then considered that as long as the dating technique measures only such photosensitive signals that were bleached at the time of deposition, reliable age estimates could be expected. A series of sun-exposures are made on different sets of aliquots and additive growth curves obtained for each of these sets as well as for the unbleached set. The equivalent dose (or palaeodose, P, as used henceforth) is determined from the intersection point of the unbleached and the bleached growth curves. In the next step the dependence of palaeodose on varying daylight exposure is examined to deduce the most appropriate bleaching condition, beyond which an overestimation of the age would occur (Fig. 1). Further understanding of the appropriate bleaching conditions were found by Berger and Lutenauer (1987) who measured the net sun spectra in turbid water (~ 500 nm to ~ 690 nm) and based on this suggested that the wavelength < 550 nm and > 700 nm should be blocked during laboratory photobleaching. This can be achieved by filtering the daylight through a combination of Schott OG 570 and KG 5 filters.

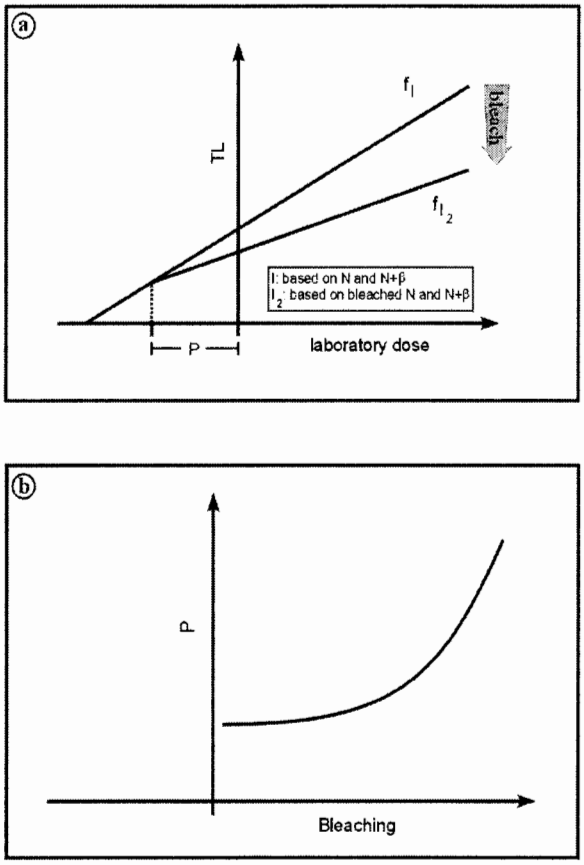

Figure1.

(a) Diagram for P determination in the partial bleach technique used in thermoluminescence dating.

(b) Expected behaviour of palaeodose with bleaching using the partial bleach technique. The palaeodose estimate will increase after the laboratory photobleaching exceeds the depositional photobleach level.

Development of optical dating with direct measurement of the easily bleached component brought the optimism that more sediments of different depositional environments could be dated, than was possible with TL (Huntley *et al.*, 1985; Hütt *et al.*, 1988). However, results of insufficient bleaching of OSL in specific situations has been reported, for example by Duller (1994), Lang (1994), Li (1994) and Rhodes and Pownell (1994). Fuller *et al.* (1994) extended the concept of restricted spectrum bleaching and the partial bleach method in TL dating to infra-red stimulated luminescence to examine deposits from the river Danube. However, from a simulation experiment it was concluded that the partial bleach methodology was inappropriate for IRSL. An alternative approach was suggested by Aitken and Xie (1992), who conceptualised that the total signal comprised an 'easy-to-bleach' and a 'hard-to-bleach' component. The authors used a 'subtraction technique' to obtain the rapidly bleaching component. To achieve this, the 'late light' of each of the shine down curves (i.e. signal appearing after a long shine down) was subtracted from the 'early light' (signals at the early intervals of the shine down). The palaeodose is then determined using the additive dose method but on the rapidly bleaching component only.

We discuss here a simple technique to conduct a partial bleach analysis in optical dating which allows for probing the most photosensitive signal and uses only simple IRSL shine down curves. The new technique comprises construction of a series of partial bleach growth curves for a sample to estimate the dependence of the palaeodose (P) with increasing optical stimulation. A somewhat similar approach was employed by Spooner *et al.* (1990) for a well bleached sample. In the following the basic philosophy of the technique is presented along with the results on sediments of different depositional environments.

The technique

In the conventional partial bleach experiment a minimum of two sets of growth curves are constructed (Fig. 1). These are,

(1) a growth curve based on natural and natural + additive doses and,

(2) a second growth curve based on an identical set of aliquots but with an additional treatment of photobleaching.

Extrapolation of the two curves and the determination of their intersection point provides the paleodose P. In the present approach, the IRSL shine down curves are analysed and IR stimulation itself substitutes for optical bleaching. The intensity $I_{\Delta t_0}$ of the first interval Δt_0 of stimulation is taken to represent the natural (unbleached) signal. The intensity of all subsequent shine down intervals are considered as photobleached signal i.e. $I_{\Delta t_1}$ ... $I_{\Delta t_n}$. (Fig. 2), with increasing photobleach as stimulation proceeds. A set of partial bleach growth curves are then constructed for different intervals using the first interval as the natural additive growth curve (i.e. $f(\Delta t_0)$) and the subsequent intervals as the photobleached ones (i.e. $f(\Delta t_1)$, $f(\Delta t_2)$,..... $f(\Delta t_n)$). P is estimated from the intersection points of the growth curves, i.e. P_1 from the intersection of $f(\Delta t_0)$ and $f(\Delta t_1)$, P_2 from the intersection of $f(\Delta t_0)$ and $f(\Delta t_2)$, ... and P_n from the intersection of $f(\Delta t_0)$ and $f(\Delta t_n)$. We call this approach the 'differential partial bleach' (DPB)

approach. In a similar approach Aitken and Xie (1992) suggested to use the subtraction technique where the difference of $I_{\Delta t_0}$ and $I_{\Delta t_n}$ is plotted to obtain the equivalent dose.

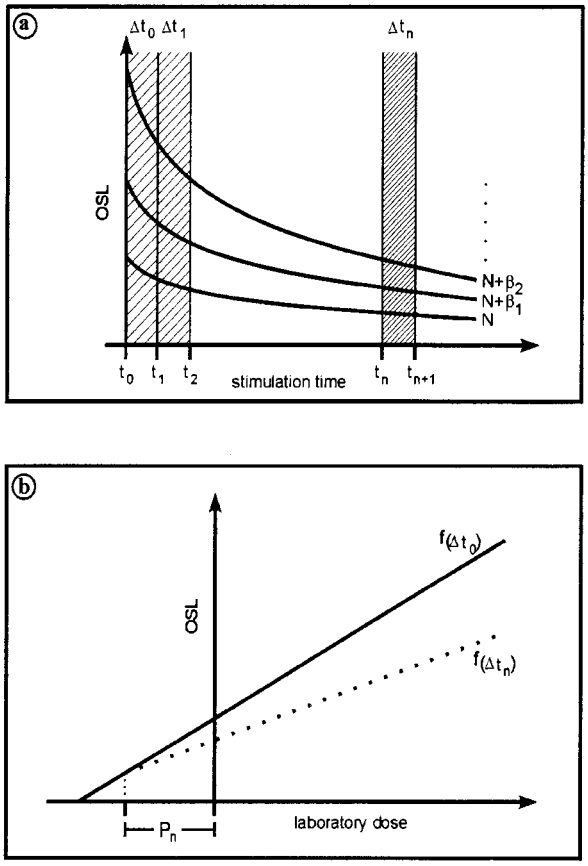

Figure 2.

(a) Schematic of the DPB approach. The intensity $I_{\Delta t_0}$ of the first interval Δt_0 of stimulation is taken to represent the unbleached (natural) signal. The intensity of all subsequent shine-down intervals are considered as equivalent to laboratory bleached i.e. $I_{\Delta t_1} \cdots I_{\Delta t_n}$.

(b) Growth curves are constructed for each interval and a palaeodose (P) is estimated - as in conventional TL partial bleach technique - at the intersection of the growth curves of unbleached and subsequent bleached intervals.

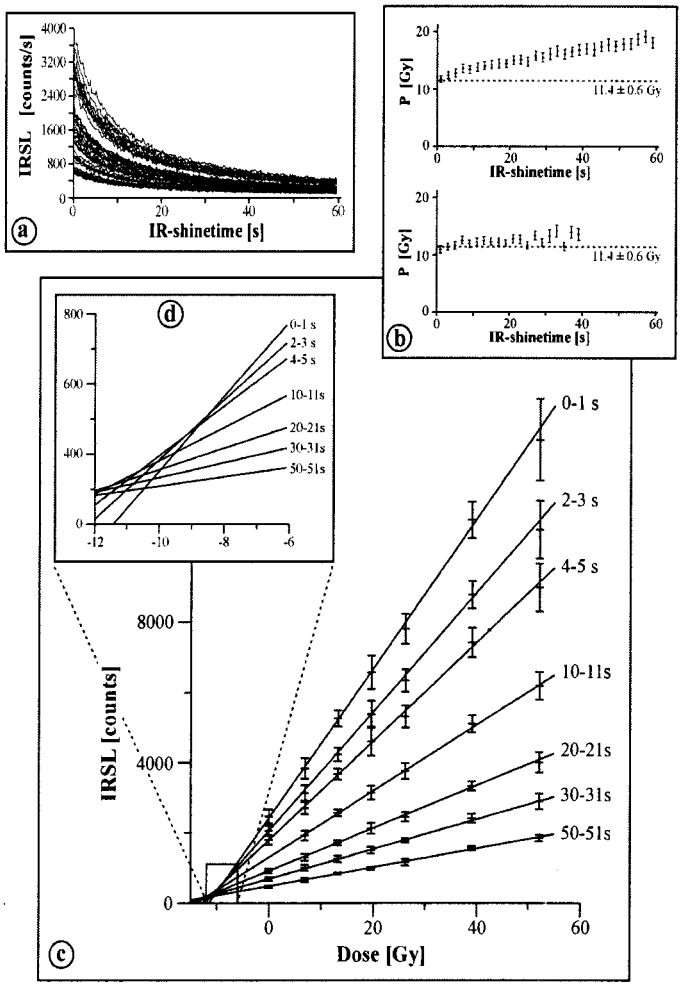

Figure 3.

(a) Shine down curves for sample HDS-180. IRSL in counts per s is plotted versus stimulation time for natural and additive dosed aliquots.

(b) Shine plots for sample HDS-180: P in Gy is plotted versus stimulation time. The upper plot shows P-values obtained using the conventional additive dose technique. The lower plot shows P-values obtained using the additive dose technique after subtraction of the 'late light' (mean signal in the interval 50 s to 60 s) The dashed lines are plotted at the additive P value obtained for the first s of stimulation (11.4 ± 0.6 Gy). No palaeodose plateau is seen.

(c) Dose response for selected intervals: integral IRSL in counts is plotted versus applied laboratory dose in Gy for different stimulation intervals (as labelled). Extrapolated lines are shown for each interval. For clarity, dose response for interval 1-2 s has been omitted.

(d) Enlargement from Fig. 2 (c): The region of intersection of the extrapolated lines is shown.

The samples

A series of silty samples from different depositional environments i.e. (a) fluvial deposits (overbank sediments), (b) colluvial deposits, and (c) aeolian deposits were investigated. Such a choice was made to examine the applicability of the present approach to samples derived from different depositional bleaching environments. It is expected that the present technique would provide an age similar to that of the conventional additive dose IRSL technique for a well bleached aeolian sample and that it should provide ages similar to that of the subtraction technique for sufficiently bleached colluvial samples. On the other hand, it should produce substantially improved ages (i.e. consistent with age controls) in case of poorly bleached proximally transported fluvial sediments. The details of samples and their depositional environments are presented below.

Fluvial deposits (Samples HDS-178 to HDS-184, MAU-EB-4 and MAU-EB-7).

All samples originate from the floodplain of the Elsenz-river near Heidelberg, Germany. These sediments consist of reworked loess, deposited as overbank sediments during floods. Samples HDS-178 to HDS-184 were recovered by drilling immediately besides the present day river channel near the town of Wiesenbach. A chronological framework for the construction of the Elsenz floodplain is provided by Barsch *et al.* (1993). Previous IRSL-studies of floodloam from besides the channel suggested very poor or no bleaching of the mineral grains at deposition (Lang, 1994). Samples MAU-EB-4 and MAU-EB-7 were taken from the floodplain at a construction site near the town of Mauer (Lang, 1996). MAU-EB-4 was taken from near the river channel, and MAU-EB-7 from the distal part of the floodplain. Radiocarbon ages on associated wood and land-snail samples provides following time frame: AD 1446-1621 for MAU-EB-4 and AD 390-530 for MAU-EB-7 (calibrated using Stuiver and Reimer, 1993).

Colluvial deposits (Samples RÖM-1 to RÖM-5)

A set of colluvial sediment samples from Wiesenbach (SW Germany) were taken. The colluvial sequence lies unconformably above a loess horizon and was deposited in response to the construction of a 'dam', such that the material further uphill that was eroded was trapped until filling of the dam was complete. Further details and results of IRSL analysis of these samples using the 410 nm emission and the subtraction technique of Aitken and Xie (1992) can be found in Lang and Wagner (1997).

Aeolian Sediment (Sample RÖM 10)

A sample of Late Würmian pristine loess was also taken at Wiesenbach (see above, detailed description in Lang and Wagner, 1997). Sedimentological characteristics and stratigraphy in the region suggest that the loess should have been deposited after the last glacial maximum. The youngest loess known in this region was laid down 14 to 15 ka ago (Zöller, 1994). Thus the sedimentation age of the sample can be bracketed to 22 to 15 ka.

Measurements

Experimental procedures *viz.* sample preparation, P and dose rate determination are described by Lang *et al.* (1996). Typically 40 - 60 shine down curves were recorded at room temperature for the paleo-dose estimation. A Risø reader TL-DA-12 (Bøtter-Jensen *et al.*, 1991) equipped with an EMI 9635Q photomultiplier and TEMT 484 diodes for stimulation (880 Δ 80 nm) was employed. The net IR power at the sample was ~40 mW/cm^2. Following Krbetschek *et al.*, (1996) the IRSL detection was restricted to 390 - 450 nm. For the construction of growth curves, typically 10 'natural' discs and 6 groups of artificially dosed discs (5 each) were measured. These satisfied the criterion for reducing the error in palaeodose to an optimum level (Felix and Singhvi, 1997). A ^{90}Sr/^{90}Y β-source (dose rate ~1 Gy/min) was used for artificial dosing and preheating of 220°C for 5 min was applied to all samples. No corrections for thermal transfer effects, such as were made by Huntley and Clague (1996), nor of the type made, for example, by Aitken and Xie (1992) and Rees-Jones and Tite (1994). Recent studies by us on mineral separates indicate that this correction may not be significant for samples with P values in excess of half a Gy. Data handling was done using G. Duller's *analyse* software. For regression analysis and calculation of intersection points the commercial software package by *Jandel Scientific* was used. In the error estimation, a weightage proportional to variance and error propagation according to the Gaussian error propagation law were applied. Dose rates were calculated from a combination of data from alpha-counting, beta-counting and high resolution low level gama ray-spectrometry (Lang *et al.*, 1996). In none of the samples was radioactive disequilibrium detected.

Results and discussion

A typical data set for a fluvial sample is provided in Fig. 3. Fig. 3a provides the shine down curves, Fig. 3b provides the shine plots using the conventional additive and late light subtraction techniques and dose response curves for different intervals are plotted in Fig. 3c. The inset (Fig. 3d) shows the different equivalent doses obtained from successive time intervals suggesting the presence of signals of different photo bleachability.

Table 1 provides the P estimates based on the new technique along with the result of conventional IRSL additive dose analysis. P estimated based on late light subtraction, the IRSL intensity in interval 1-2 sec. taken as 'late light' is also provided for comparison. The 'expected P' is calculated using the dose rate of the sample and the estimated age of the sample based on the contextual and stratigraphical information and on the radiocarbon ages. Fig. 4 provides a comparison of the P-values from the DPB analysis and P-values from conventional additive dose analysis.

(a) ***Fluvial deposits*** - Floodloam sequence HDS-178 to HDS-184. In this series, the differential partial bleach technique provides a substantial improvement compared to the standard IRSL additive dose and subtraction procedures using 50-60 s as the late light. The DPB values show a good concordance with the expected values. The only exceptions are HDS-180 and HDS-183, where although the use of DPB technique provides an improvement, still the DPB palaeodose is overestimated compared to the expected P. This would imply that the present choice of analysis intervals are still too long. The examination of sub-second intervals however was limited by the photon counting statistics and will have to await higher efficient measurement devices. Two fluvial samples from the other locality (MAU-EB) show differing results. Whereas P values calculated for MAU-EB-4 show a trend similar to HDS-180 and HDS-183, P values calculated for MAU-EB-7 (the distal sediment) are the same within error limits and fit to the expected P. The conventional additive dose P value is higher.

(b) ***Colluvial deposits***: For all the samples P values calculated are the same within error limits and fit well to the known values. The exceptions are the conventional additive dose P.

(c) ***Aeolian deposits***: All P-values determined for RÖM 10 are the same within the limits of error, again with the exception of the conventional additive dose P.

From these results two groups of samples can be distinguished. Group (1) shows a trend towards lower P values when analysing earlier intervals and therefore exhibit significant improvements with the use of the DPB-technique. Group (2) has all P values that are identical and fall within the error limits, except the conventional additive P estimates. Group (2) comprises the well bleached aeolian loess, reworked sediments like the RÖM-1 to RÖM-5 which also behave like well bleached sediments. Here the DPB estimates are comparable to other estimates. The higher conventional additive P is possibly due to the hard to bleach component of the blue emission (Rieser *et al.*, 1997; Lang and Wagner, 1997).

In view of the fact that, an optical exposure can be finely tuned in respect of the flux, wavelength and duration, the present approach permits the growth curves for situations where the signal sampling interval Δt_0 can be made as small as possible and the flux for IR-simulation may be reduced to the lowest possible level. It is considered that the approach is likely to be limited only by

(1) photon counting statistics
(2) photobleaching during sample preparation (if any), and
(3) signal loss during short shine normalisation runs.

Effects due to scattered illumination light into the detection optics, Raman scattering, thermal transfer and photomultiplier dark counts are common to both the intervals Δt_0 and Δt_n and consequently it can be reasonably expected that they will get eliminated automatically.

The technique implicitly assumes the presence of a spectrum of bleachability in the OSL signal. This is the case for polymineral fine grain samples. The technique's utility for coarse grains (and single grains) remains to be investigated. The method should compliment the single grain technique in the sense that while the single grain technique aims to locate the most bleached grains in a heterogeneously bleached ensemble of grains, the DPB method looks for the most rapidly bleachable signal in such an ensemble.

***Table 1**: P estimates for the different approaches used. Sample No., sediment type, sampling depth (in case of the fluvial sequence) are also listed. All P values are in Gy.*

		P	P	P	P	P	P	P	P
	Technique:	(convent.)	(subtr.)	(subtr.)	(DPB)	(DPB)	(DPB)	(DPB)	'expected'
	Interval:	0-1s	(50-60s)	(1-2s)	20-21s	10-11s	2-3s	1-2s	
Sample	Sed.-type								
HDS178	Floodloam (70 cm)	6.1± 0.3	5.3±0.3	3.1±0.4	5.0±0.2	4.3±0.3	3.7±0.2	1.3±0.3	1-2
HDS179	floodloam (140 cm)	6.6±0.2	5.7±0.2	1.7±0.4	5.8±0.3	6.5±0.4	4.50.3±	2.4±0.4	2-3
HDS180	floodloam (260 cm)	11.4±0.6	10.6±0.5	6.8±0.5	9.9±0.8	9.5±0.7	8.5±0.6	6.6±0.5	2-5
HDS181	floodloam (365 cm)	5.1±0.3	4.5±0.2	3.3±0.6	4.4±0.4	4.4±0.4	4.3±0.3	3.8±0.3	3-7
HDS182	floodloam (390 cm)	5.0±0.3	4.5±0.3	4.1±0.5	4.6±0.5	4.4±0.4	4.3±0.4	4.0±0.3	3-8
HDS183	floodloam (650 cm)	36.5±1.7	35.4±1.7	33.2±1.9	35.2±2.2	34.6±2.4	31.2±2.2	35.9±5.6	10-20
HDS184	floodloam (680 cm)	17.3±1.0	16.3±1.1	16.9±3.1	16.1±1.2	16.0±1.3	16.9±1.4	15.3±1.4	12-25
MAU EB 4	floodloam	24.0±1.5	22.5±1.5	16.3±1.4	21.1±1.5	20.1±1.5	17.0±1.4	15.9±1.4	1.5-2.5
MAU EB 7	floodloam	4.6±0.2	4.3±0.2	4.7±0.6	4.2±0.2	4.1±0.2	3.9±0.2	3.9±0.2	4.5-6.0
RÖM 1	colluvium	4.2±0.3	2.0±0.1	2.0±0.5	2.1±0.2	2.0±0.2	2.2±0.2	2.2±0.2	0-4
RÖM 2	colluvium	5.2±0.2	2.6±0.1	1.4±0.2	2.4±0.3	2.4±0.2	2.2±0.2	2.1±0.2	0-4
RÖM 3	colluvium	5.5±0.4	3.3±0.2	3.8±0.5	3.3±0.4	3.4±0.4	3.8±0.4	4.0±0.4	2-6
RÖM 4	colluvium	8.4±0.4	8.0±0.4	7.0±1.3	7.9±0.5	7.8±0.5	8.2±0.5	7.4±0.5	6-11
RÖM 5	colluvium	14.2±1.2	11.7±1.0	10.7±2.2	9.9±1.2	11.3±1.3	11.7±1.4	12.0±1.3	7-12
RÖM 10	loess	69.6±2.7	62.4±2.2	56.5±5.8	59.7±2.8	57.8±3.0	56.8±2.9	57.7±3.1	50-75

(convent.): P is determined using the 'conventional' additive dose technique and the IRSL signal of the first second of stimulation (0-1 s intervals).

(subtr.): Subtraction technique P estimates using the integral 50-60 s or 1-2 s (as indicated) for determination of the 'late light'.

(DPB): P estimates were determined using the differential partial bleach technique as described in the text. P was calculated from the intersection point of the growth curve constructed for the first interval of stimulation and the growth curve of the specified interval.

'expected': P is calculated using calibrated ^{14}C ages, stratigraphy of the sediments and dose rate determinations as described in the text.

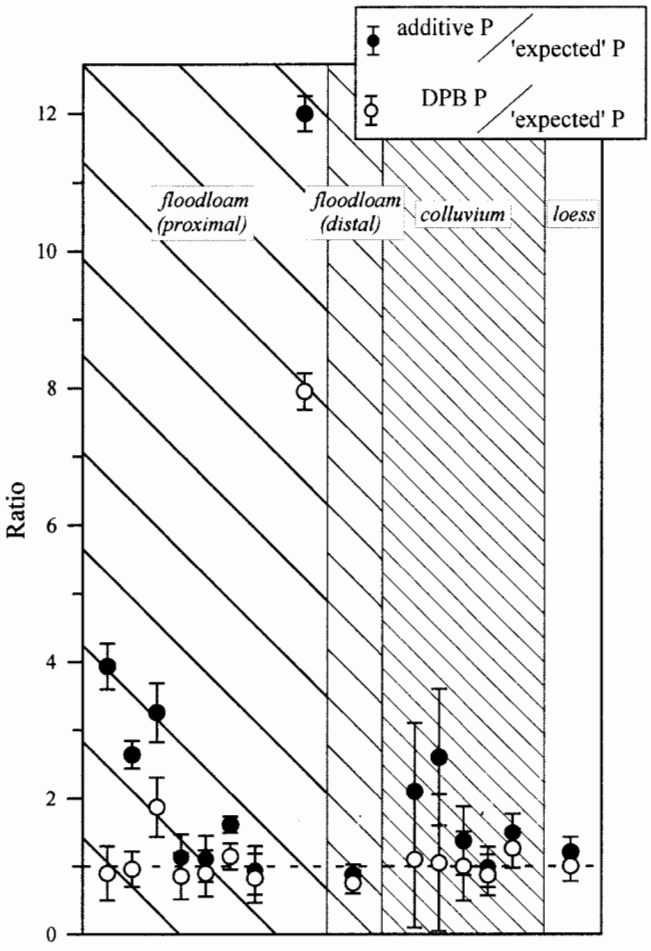

Figure 4.
Comparison of the P estimates from samples of different depositional environments using the DPB and the 'conventional' additive dose techniques. The results are presented as ratios. P estimates for DPB were obtained from the intersection point of the 0-1 s growth curve and the 1-2 s growth curve. The samples are (from left to right):

floodloam (proximal): *HDS 178, HSD 179, HDS 180, HDS 181, HDS 182, HDS 183, HDS 184, MAU EB 4*

floodloam (distal): *MAU EB 7*

colluvium: *RÖM 1, RÖM 2, RÖM 3, RÖM 4, RÖM 5*

loess: *RÖM 10*

Conclusions

The consistency of results obtained for a variety of sediments from different depositional environments enables a reasonable conclusion that the DPB technique will prove useful for the samples that experienced very limited daylight exposure prior deposition. Despite the pessimism of Fuller *et al.* (1994), it appears that the partial bleach approach as described here at any rate is not only useful but is perhaps essential when dating sediments which may be poorly bleached. This approach, as also the case with the single grain analysis being developed by e.g. Lamothe *et al.* (1994) and Murray and Roberts (1997) or single aliquot technique (e.g. Duller, 1995), should imply a significant advance in the dating of fluvial, colluvial and glacial/nival deposits.

As of now we consider the limiting factors to be only the photon counting statistics when dealing with sub-second intervals, and the luminescence intensity lost in short shine normalisation procedures. For the moment the technique should prove useful especially in the case of 'bright' samples. For polymineral samples and low P values the DPB technique is limited until more efficient light measurement devices are available. As for now, using a different detection window (560nm; Krbetschek *et al.*, 1996) may reduce the problems due to the relative large scatter in IRSL and in addition, may probe a more easy to bleach emission. However, the long-term stability of this signal is yet to be demonstrated. It would be interesting to see to what extent the technique is effective with using visible wavelengths for stimulation and to samples other than polymineral. It would also be of interest to examine cases where samples show a complex shine down curve - rising initially and decaying subsequently (Rieser et al. 1997) and to apply the DPB technique to samples artificially partially bleached in the laboratory.

Acknowledgements

We respectfully dedicate this contribution to the memory of Vagn Mejdahl who contributed immensely to the growth of TL and OSL dating.

This work was accomplished during the stay of AKS at the Institut fur Angewandte Physik on a Deutsche Forschungsgemeinschaft fellowship. AKS thanks the Institut für Angewandte Physik and its Director Prof. W. Stolz for providing the facilities for this work. We are indebted to Prof. G.A. Wagner for his kind interest and encouragement. We thank U. Rieser, and R. Kuhn for interesting discussions and are grateful to Dr. S. Stokes and Dr. E. Rhodes for their constructive suggestion on an earlier version of this manuscript. We incorporated some of the suggestions of an anonymous reviewer when an earlier version of this paper was being considered by another journal. We thank Prof. M.J. Aitken for his critical and helpful review of the manuscript. This work is a contribution to IGCP-349 and to DST (India), project on Thar Desert (ESS/CA/A3-08/92).

References

Aitken M.J. and Xie J. (1992) Optical dating using infra-red diodes: young samples. *Quat. Sci. Revs.* **11**, 147-152.

Barsch D., Mausbacher R., Schukraft G. and Schulte A. (1993) Die Änderung des Naturraumpotentials im Jungneolithikum des nordlichen Kraichgaus dokumentiert in fluvialen Sedimenten. *Z. Geomorph. N.F. Suppl.* **93**, 175-187.

Berger G.W. (1988) Dating Quaternary events by luminescence. In Easterbrook D.J. (ed.), Dating Quaternary Sediments. *Geol. Soc. Am. Special Paper* **227**, 13-50.

Berger G.W. (1990) Effectiveness of natural zeroing of the thermoluminescence in sediments. *J. Geophys. Res.* **95**, 12,375-12,397.

Berger G.W. and Luternauer J.L. (1987) Preliminary fieldwork for thermoluminescence dating of Fraser river delta, British Columbia. *Geol. Survey of Canada paper* **87-1A**, 901-904.

Bøtter-Jensen L., Ditlefsen C. and Mejdahl V. (1991) Combined OSL (infrared) and TL studies of feldspars. *Nucl. Tracks Radiat. Meas.* **18**, 257-263.

Duller G.A.T. (1994) Luminescence dating of poorly bleached sediments from Scotland. *Quat. Geochronology (Quat. Sci. Revs.)* **13**, 521-524.

Duller G.A.T. (1995) Luminescence dating using single aliquots: methods and applications. *Radiat. Meas.* **24**, 217-226.

Felix, C. and Singhvi, A.K. (1997) Study of non-linear luminescence dose growth curves for the estimation of paleodose in luminescence dating: Results of Monte Carlo Simulation. *Rad. Meas.* **27**, 599-609.

Fuller I.C., Wintle A.G. and Duller G.A.T. (1994) Test of the partial bleach methodology as applied to the infra-red stimulated luminescence of an alluvial sediment from Danube. *Quat. Sci. Revs.* **13**, 539-543.

Huntley, D.J. (1985) On the zeroing of thermoluminescence in sediments. *Physics and Chemistry of Minerals* **12**, 122-127.

Huntley, D.J. and Clague, J. J. (1996) Optical dating of tsunami laid-sands. *Quat. Res.* **46**, 127-140.

Huntley, D.J., Godfrey Smith, D.I. and Thewalt, M.L.W. (1985) Optical dating of sediments. *Nature* **313**, 105-107.

Hütt G., Jaek I. and Tchonka J. (1988) Optical dating: K-feldspars optical response stimulation spectrum. *Quat. Sci. Rev.* **7**, 381-386.

Krbetschek M.R., Rieser U. and Stolz W. (1996) Optical dating: Some luminescence properties of natural feldspars. *Radiation Protection Dosimetry* **66**, 407-412.

Lamothe M., Balescu S. and Auclair M. (1994) Natural IRSL intensities and apparent luminescence ages of single feldspar grains extracted from partially bleached sediments. *Radiat. Meas.* **23**, 555-561.

Lang A. (1994) Infra-red stimulated luminescence dating of Holocene reworked silty sediments. *Quat. Sci. Revs.* **13**, 525-528.

Lang A. (1996) *Die Infrarot Stimulierte Lumineszenz als Datierungsmethode fur holozane Lossderivate.* Heidelberger Geographische Arbeiten **101**, 137pp.

Lang A. and Wagner G.A. (1997) Infra-red stimulated luminescence dating of Holocene colluvial sediments using the 410 nm emission. *Quat. Geochronology (Quat. Sci. Revs.)* **16**, 393-396.

Lang A., Lindauer S., Kuhn R. and Wagner G.A. (1996) Procedures used for optically and infra-red stimulated luminescence dating of sediments in Heidelberg. *Ancient TL* **14**, 7-11.

Li S.-H. (1994) Optical dating: Insufficiently bleached sediments. *Radiat. Meas.* **23**, 563-568.

Murray, A.S. and Roberts, R.G. (1997) Determining the burial time of single grains of quartz using optically stimulated luminescence. *Earth and Planetary Science Letters* **152**, 163-180.

Rees-Jones, J. and Tite, M. S. (1994) Recuperation of IRSL after bleaching and consequences for dating young sediments. *Radiat. Meas.* **23**, 569-574.

Rieser U., Hütt G., Krbetschek M.R. and Stolz W. (1997) Feldspar IRSL emission spectra at high and low temperatures. *Radiat. Meas.* **27**, 273-278.

Rhodes E.J. and Pownall L. (1994) Zeroing of the OSL signal in quartz from young glaciofluvial sediments. *Radiat. Meas.* **23**, 581-586.

Spooner N.A., Aitken M. J., Smith B. W., Franks M. and McElroy, C. (1990) Archaeological dating by infrared-stimulated luminescence using a diode array. *Radiat. Protection Dosimetry.* **34**, 83-86.

Stuiver M. and Reimer P.J. (1993) Extended ^{14}C data base and revised CALIB 3.0 ^{14}C age calibration. *Radiocarbon* **35**, 215-230.

Wintle A.G. and Huntley D.J. (1979) Thermoluminescence dating of a deep-sea ocean core. *Nature* **279**, 710-712.

Wintle A.G. and Huntley D.J. (1980) Thermoluminescence dating of ocean sediments. *Can. J. Earth Sci.* **17**, 348-360.

Zöller L. (1994) *Würm- und Risslöss-Stratigraphie und Thermolumineszenz-Datierungen in Süddeutschland und angrenzenden Gibieten.* Habilitationsschrift, University of Heidelberg, 174pp.

Reviewer :
Martin Aitken

Comments

1. In essence this is an extension of the subtraction method of Aitken & Xie (1992) ; it differs in the way the data are handled --- as the authors indicate. A further development that might be worth considering would be to use the successive adjacent time intervals instead of always using the first time interval ; this should give better separation of components of differing bleachability though of course these harder-to-bleach components will have suffered a minor amount of bleaching. However, in terms of obtaining the palaeodose for the easiest-to-bleach component there would be no advantage.

2. Because the same data are used for each it is to be expected that the palaeodose obtained by subtraction using a given time interval for the late-light will be the same as that obtained by DPB technique for that interval. The Table enables this comparison to be made for the 1-2 s interval and it will be seen that there is agreement except in respect of HDS178 and RÖM 2 ; these are only two of several low palaeodose samples, and also since the discrepancies are in opposite sense, this feature does not seem likely to be indicative of a systematic effect associated with low palaeodose.

3. I disagree with the authors' expectation that the technique will eliminate thermal transfer effects. My own expectation, consistent with observations (unpublished) I made some years ago using green-light stimulation, is that the shine-down curve for the transferred component will have the same shape as that of the dating signal (the « natural ») ; hence the transferred component will constitute the same percentage of the signal for all time intervals and this will lead to an overestimation of palaeodose by that percentage irrespective of whether the DPB or the subtraction technique is used. Of course for many samples the transfer component is, in any case, barely significant.

Thesis abstract

Thesis title: The form of the optically stimulated luminescence signal of quartz : implications for dating
Author: Richard Bailey
Examined by: Prof. Ann Wintle and Dr Richard Templer
Awarded by: London University

Optically stimulated luminescence (OSL) signals measured from natural sedimentary quartz vary significantly in form depending upon a variety of factors, including the irradiation/illumination/thermal history of the sample and laboratory measurement conditions. An attempt has been made in this thesis to understand the factors responsible for the observed variation in decay form and to exploit this understanding for the benefit of optical dating. The origin of the observed non-exponential OSL decay and the issue of single versus multiple signal components were found to be of paramount importance.

Empirically constrained analytical and numerical modelling of charge transfer (through the conduction band) within an electronic system analogous to that of quartz indicates that the OSL stimulated from a single trap is expected to decay exponentially (to a very good approximation) with time. The empirically observed OSL signal (measured at 160°C) was found to be adequately fitted using a sum of two exponentials, the 'fast' and 'medium' components, plus a third non-exponential ('slow') component, best fitted using a ln(t) decay in most cases.

Isothermal decay analysis suggests that both the fast and medium components are associated with the TL region centred on 330°C. The third 'slow' component signal is extremely thermally stable, present after heating to 500°C. A thermo-optically stimulated direct donor-acceptor recombination pathway was inferred for the slow component. Further differences between each OSL component were observed in, for example, dose response and thermal assistance in detrapping. The conclusion drawn was that the observed OSL most likely comprises three physically distinct signals.

Two aspects of quartz optical dating that may benefit from analysis of the identified signal components have been addressed in some detail; these are (i) the identification of partially bleached sediments, and (ii) the possible extension of the dateable age range.

Announcement

LED99

9th International Conference on Luminescence and Electron Spin Resonance Dating

6-10 September 1999

ROME-ITALY

The 9th International Conference on Luminescence and Electron Spin Resonance Dating (LED99) will be held in Rome at the Complesso Monumentale del San Michele a Ripa from Monday 6th to Friday 10th September 1999.

LED99 will gather experts from around the world in fields of Luminescence and Electron Spin Resonance Dating. The topics range from fundamental studies of the basic physical phenomena to dosimetry, advances in equipment technology and applications of the dating techniques in Quaternary researches, accident dosimetry, archaeology and history of art.

Proceedings

Proceedings will be refereed and published in Quaternary Geochronology and Radiation Measurements.

Further information

Enquiries for further information should be addressed to:
Dr. Emanuela Sibilia - Dipartimento di Scienza dei Materiali, via Emanueli, 15 - 20126 Milano
TEL. +39+2+66174.165 (.166.167)
FAX +39+2+66174400
E-MAIL sibilia@mater.unimi.it
WEB SITE http//www.mater.unimi.it/LED99

Bibliography

(From 1 April 1998 to 1 October 1998) Compiled by Ann Wintle

Aitken M.J. (1988) Introduction to Optical Dating. Oxford University Press, Oxford.

Balescu S., Breton L.F., CoqueDelhuille B. and Lamothe M. (1998) Luminescence dating of flash flood deposits: a new approach for the chronological study of ancient irrigation perimeters in southern Yemen. Comptes Rendus de l'Academie des Sciences Serie II 327, 31-37.

Bryant E.A. and Price D.M. (1997) Late Pleistocene marine chronology of the Gippsland Lakes region, Australia. Physical Geography 18, 318-334.

Bryant E.A., Young R.W., Price D.M. and Wheeler D.J. (1997) The impact of tsunami on the coastline of Jervis Bay, Southeastern Australia. Physical Geography 18, 440-459.

Clark R.J. and Bailiff I.K. (1998) Fast time-resolved luminescence emission spectroscopy in some feldspars. Radiation Measurements 29, 553-560.

Clarke M.L. and Rendell H.M. (1998) Climate change impacts on sand supply and the formation of desert sand dunes in the south-west U.S.A. Journal of Arid Environments 39, 517-531.

Correcher V. and Delgado A. (1998) On the use of natural quartz as transfer dosemeter in retrospective dosimetry. Radiation Measurements 29, 411-414.

de Meijer R.J. (1998) Heavy minerals: from 'Edelstein' to Einstein. Journal of Geochemical Exploration 62, 81-103.

Franklin A.D. (1998) A kinetic model of the rapidly bleaching peak in quartz thermoluminescence. Radiation Measurements 29, 209-221.

Frechen M. and Dodonov A.E. (1998) Loess chronology of the Middle and Upper Pleistocene in Tadjikistan. Geol. Rundsch. 87, 2-20.

Fukuchi T. and Imai N. (1998) Resetting experiment of E' centres by natural faulting - the case of the Nojima earthquake fault in Japan. Quaternary Geochronology (Quaternary Science Reviews) 17, 1063-1068.

Grün R. (1998) Reproducibility measurements for ESR signal intensity and dose determination: high precision but doubtful accuracy. Radiation Measurements 29, 177-193.

Guibert P., Bechtel F., Schvoerer M., Muller P. and Balescu S. (1998) A new method for gamma dose-rate estimation of heterogenous media in TL dating. Radiation Measurements 29, 561-572.

Hashimoto T., Yasuda K., Sato K., Sakaue H. and Katayama H. (1998) Radiation-induced luminescence images and TL-property changes with thermal annealing treatment on Japanese twin quartz. Radiation Measurements 29, 493-502.

Hatte C., Fontugne M., Rousseau D.D., Antoine P., Zöller L., Tisnerat-Laborde N. and Bentaleb I. (1998) Delta 13C variations of loess organic matter as a record of the vegetation response to climatic changes during the Weichselian. Geology 26, 583-586.

Jaek I., Hütt G., Vasilchenko E., Nagirnyi V., Zazubovich S. and Seeman V. (1997) Luminescence and microstructure of Ga, In and Tl centres in laboratory-doped natural feldspars. Journal of Luminescence 72-74, 681-683.

Knight J., Orford J.D., Wilson P., Wintle A.G. and Braley S. (1998) Facies, age and controls on recent coastal sand dune evolution in North Norfolk, Eastern England. Journal of Coastal Research 26, 154-161.

Kuzucuoglou C., Parish R. and Karabiyikoglu M. (1998) The dune systems of the Konya Plain (Turkey): their relation to environmental changes in Central Anatolia during the Late Pleistocene and Holocene. Geomorphology 23, 257-271.

Laurent M., Falgueres C., Bahain J.J., Rousseau L. and van vliet Lanoe B. (1998) ESR dating of quartz extracted from Quaternary and Neogene sediments: method, potential and actual limits. Quaternary Geochronology (Quaternary Science Reviews) 17, 1057-1062.

McFadden L.D., McDonald E.V., Wells S.G., Anderson K., Quade J. and Forman S.L. (1998) The vesicular layer and carbonate collars of desert soils and pavements: formation, age and relation to climate change. Geomorphology 24, 101-145.

McFee C.J. (1998) The measurement of single grain IRSL EDs using an imaging photodetector. Quaternary Geochronology (Quaternary Science Reviews) 17, 1001-1008.

Michab M., Feathers J.K., Joron J.L., Mercier N., Selos M., Valladas H., Valladas G., Reyss J.L. and Roosevelt A.C. (1998) Luminescence dates for the paleoindian site of Pedra Pintada, Brazil. Quaternary Geochronology (Quaternary Science Reviews) 17, 1041-1046.

Molodkov A., Dreimanis A., Aboltins O. and Raukas A. (1998) The ESR age of Portlandia Arctica shells from glacial deposits of central Latvia: an answer to a controversy of the age and genesis of their enclosing sediments. Quaternary Geochronology (Quaternary Science Reviews) 17, 1077-1094.

Murray A.S. and Roberts R.G. (1998) Measurement of the equivalent dose in quartz using a regenerative-dose single-aliquot protocol. Radiation Measurements 29, 503-515.

Oczkowski H.L. and Przegietka K.R. (1998) TL dating of young aeolian deposits from Kepa Kujawska. Radiation Measurements 29, 435-439.

Olley J.M., Caitcheon G. and Murray A. (1998) The distribution of apparent dose as determined by optically stimulated luminescence in small aliquots of fluvial quartz: implications for dating young sediments. Quaternary Geochronology (Quaternary Science Reviews) 17, 1033-1040.

Ono Y., Naruse T., Ikeya M., Kohno H. and Toyoda S. (1998) Origin and derived courses of eolian dust deposited during marine isotope stage 2 in East Asia, suggested by ESR signal intensity. Global and Planetary Change 18, 129-135.

Prescott J.R., Scholefield R.B. and Franklin A.D. (1995) Three-dimensional thermoluminescence spectra and their application in the study of some sedimentary quartz. Scanning Microscopy Supplement 9, 245-254.

Rogalev B., Chernov V., Korjonen K. and Jungner H. (1998) Simultaneous thermoluminescence and optically stimulated luminescence dating of Late Pleistocene sediments from Lake Baikal. Radiation Measurements 29, 441-444.

Rousseau D.D., Zöller L. and Valet J.P. (1998) Late Pleistocene climatic variations at Achenheim, France, based on a magnetic susceptibility and TL chronology of loess. Quaternary Research 49, 255-263.

Spooner N.A. (1998) Human occupation at Jinmium, northern Australia: 116,000 years ago or much less? Antiquity 72, 173-178.

Trautmann T., Krbetschek M.R., Dietrich A. and Stolz W. (1998) Investigations of feldspar radioluminescence: potential for a new dating technique. Radiation Measurements 29, 421-425.

Tveranger J., Astakhov V., Mangerud J. and Svendsen J.I. (1998) Signature of the last shelf-centred glaciation at a key section in the Pechora Basin. Journal of Quaternary Science 13, 189-203.

Urbina M., Millan A., Beneitez P. and Calderon T. (1998) Dose rate effect in calcite. Journal of Luminescence 79, 21-28.

Vaijapurkar S.G., Raman R. and Bhatnagar P.K. (1998) Sand- a high gamma dose thermoluminescence dosimeter. Radiation Measurements 29, 223-226.

van den Haute P., Vancraeynest L. and de Corte F. (1998) The Late Pleistocene loess deposits and palaeosols of eastern Belgium: new TL age determinations. Journal of Quaternary Science 13, 487-497.

Vermeersch P.M., Paulissen E., Stokes S., Charlier C., Van Peer P., Stringer C. and Lindsay W. (1998) A Middle Palaeolithic burial of a modern human at Taramsa Hill, Egypt. Antiquity 72, 475-484.

Visocekas R., Tale V., Zink A. and Tale I. (1998) Trap spectroscopy and tunnelling luminescence in feldspars. Radiation Measurements 29, 427-434.

Wintle A.G., Clarke M.L., Musson F.M., Orford J.D. and Devoy R.J.N. (1998) Luminescence dating of recent dunes on Inch Spit, Dingle Bay, southwest Ireland. The Holocene 8, 331-339.

Ye Y.G., Diao S.B., He J., Gao J.C. and Lei X.Y. (1998) ESR dating studies of palaeo-flow deposits in Dongchuan, Yunnan Province, China. Quaternary Geochronology (Quaternary Science Reviews) 17, 1073-1076.

Ye Y.G., Liang H.D., Diao S.B., Wang R.H., Dai C.S. and Gao J.C. (1998) Concentration of oxygen vacancies in quartz from sediments: potential for geochronometry. Quaternary Geochronology (Quaternary Science Reviews) 17, 1069-1071.